Appendix IV:

Ni and/or Co Molybdates modified by Bismuth and/or Lanthanides: Characterization and Catalytic Activity in Propane ODH
- Detailed Results -

IV. Ni and/or Co molybdates modified by bismuth and/or lanthanides: characterization and catalytic activity in propane ODH

IV.1 Characterization of bulk M-Ln(Bi)-Mo-catalysts prepared by the citrate method

IV.1.1 Thermal behaviour

Figure IV.1 displays the thermograms of Ni-La-Mo and Ni-Bi-Mo compounds as exemples. In citrate-prepared catalysts two different types of thermal degradation schemes are observed. Almost all thermograms are characterized by a progressive weight loss between 373 and 873 K. Only the TGA of M-Bi-Mo (M = Ni or Co) samples exhibit an abrupt degradation between 673 and 723 K. In consequence to these results, two different calcination conditions have been used for the citrate-prepared catalysts: 923 and 823 K in a flow of 1 $l \cdot min^{-1}$ of dry air for 20 h.

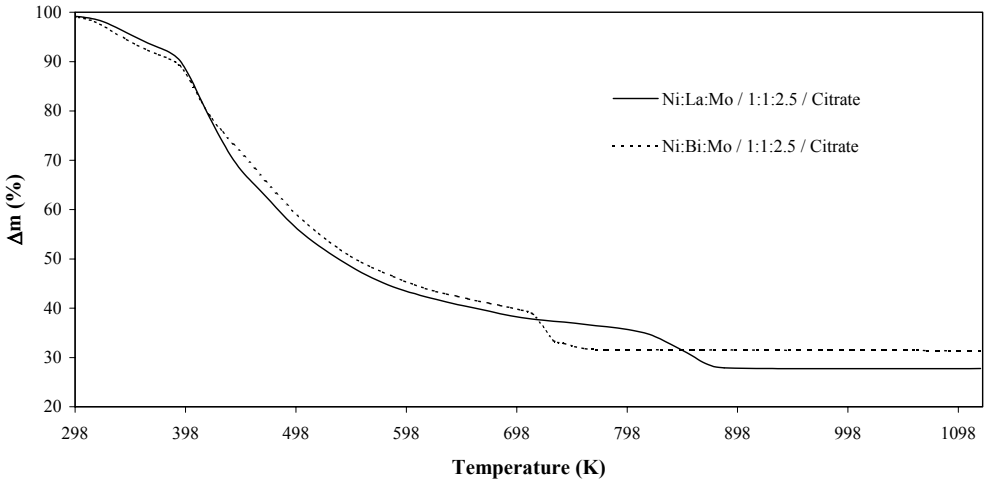

Fig. IV.1: Thermograms of Ni-La-Mo and Ni-Bi-Mo catalysts prepared by the citrate method.

IV.1.2 X-ray photoelectron spectroscopy

In all M-Ln(Bi)-Mo samples (M = Ni, Co and Ln = La, Ce, Pr, Sm, Tb), the elements are characterized by their normally expected oxidation states : Ni(II), Co(II), Mo(VI), Ln(III), Bi(III). The binding energies of the various elements were found in the following ranges : 855.3 ± 0.3 eV for Ni $2p_{3/2}$, 781.0 ± 0.1 eV for Co $2p_{3/2}$, 232.4 ± 0.2 eV for Mo $3d_{5/2}$, 159.2 ± 0.1 eV for Bi $4f_{7/2}$, 835.4 ± 0.1 eV for La $3d_{5/2}$, 933.9 ± 0.1 eV for Pr $3d_{5/2}$, 900.4 ± 0.1 eV for Ce $3d_{3/2}$, 1083.4 ± 0.2 eV for Sm $3d_{5/2}$.

Table IV.1 summarizes the experimental atomic intensity ratios measured by XPS for some citrate-prepared catalysts, which are compared with the theoretical values corresponding to the bulk composition.

In Ni-based catalysts, the experimental values of (Ni/Mo) are quite the same even if far from the theoretical ones. In general, experimental and theoretical values are closer in Co-based systems, and cobalt is more easily detected on the surface than nickel. The experimental values of (M'/Mo) (M'= Ln or Bi) in both Ni and Co-molybdates are very close.

Table IV.1: Relative atomic intensity ratios measured by XPS in M-M'-Mo (1:1:2.5) catalysts prepared by citrate method.

M = Ni, Co	**M/Mo**		**M'/Mo**		**M/M'**	
M' = La, Ce, Pr, Sm, Bi	**Exp**	**Th**	**Exp**	**Th**	**Exp**	**Th**
Ni-La-Mo	0.175	0.4	0.3	0.4	0.58	1
Ni-Ce-Mo	0.18	0.4	0.22	0.4	0.79	1
Ni-Pr-Mo	0.19	0.4	0.22	0.4	0.90	1
Ni-Sm-Mo	0.28	0.4	0.16	0.4	1.78	1
Ni-Bi-Mo	0.19	0.4	0.29	0.4	0.67	1
Co-La-Mo	0.27	0.4	0.35	0.4	0.76	1
Co-Ce-Mo	0.25	0.4	0.34	0.4	0.73	1
Co-Pr-Mo	0.45	0.4	0.29	0.4	1.57	1
Co-Sm-Mo	0.33	0.4	0.16	0.4	2.01	1
Co-Bi-Mo	0.6	0.4	0.29	0.4	1.98	1

IV.1.3 Raman spectroscopy

All citrate-prepared catalysts have been analyzed by Raman spectroscopy. These data (tables IV.3 and IV.4 for Ni- and Co- based molybdates, respectively) were interpreted by referring to the literature (103,104) and previous results we obtained for some pure phases (table IV.2).

Table IV.2: Raman data of pure phases used as references.

References	Raman shift (cm^{-1})
$La_2Mo_3O_{12}$	914-900 (vs), 841 (m), 818 (m), 783-770 (w), 741 (w), 395 (m), 354 (w), 344 (w), 327 (m), 295 (m)
$Pr_2Mo_3O_{12}$	934 (m), 915 (vs), 905 (m), 897 (m), 883 (m), 860 (m), 841 (w), 831 (w), 822 (w), 816 (m), 770 (w), 746 (w), 382 (w), 325 (w), 311 (m)
$Bi_2Mo_3O_{12}$	994 (w), 966 (m), 925 (s), 900 (vs), 857 (s), 840 (s), 815 (vs), 650 (s), 511 (m), 364 (s), 336 (w), 320 (m), 290 (w), 251 (w), 193 (s), 159 (s), 119 (m)
$Sm_2Mo_3O_{12}$	937 (s), 917-908 (vs), 894-885 (vs), 863 (s), 846 (m), 834 (m), 826 (w), 819 (m), 773 (m), 752 (m), 378 (w), 354 (m), 325 (s), 311 (s)

Table IV.3: Raman data of modified Ni-molybdates obtained by the citrate method.

Composition	Ramans shifts (cm^{-1})
Ni-La-Mo	959-945 (vs), 930.7 (m), 917 (vs), 907 (m), 892 (s), 862 (m), 822 (m), 818 (m), 772 (w), 747 (w), 705 (m), 371 (m), 324 (s), 310.3 (m)
Ni-Ce-Mo	959-948 (vs), 935 (m), 915 (vs), 897 (s), 888 (s), 879 (m), 864 (m), 846.6 (w), 838 (m), 823 (s), 808 (w), 772 (w), 746 (w), 703 (m), 384 (m), 369 (m), 347 (w), 338 (w), 325 (m), 307 (m)
Ni-Pr-Mo	959-945 (vs), 933 (m), 915 (vs), 902 (s), 892 (s), 877 (w), 859 (m), 840 (w), 830 (w), 823 (s), 814 (w), 770 (w), 744 (w), 705 (m), 387 (m), 370 (m), 352 (w), 339 (w), 328.6 (w), 311 (s)
Ni-Sm-Mo	960 (vs), 913-897 (vs), 839 (w), 815 (w), 779 (w), 705 (m), 414 (w), 386 (m), 367 (w), 353 (w), 325 (w), 309 (w)
Ni-Tb-Mo	960-947 (vs), 913-900 (vs), 844 (w), 821 (m), 782 (m), 742 (w), 705 (m), 404 (w), 367 (w), 349 (w), 329(w), 300 (m)
Ni-Bi-Mo	993 (w), 959 (vs), 929 (m), 915 (s), 899 (s), 856 (w), 839 (w), 814 (s), 703 (w), 649 (w), 507 (w), 413 (w), 388 (w), 364 (s), 317 (w) 247 (w), 192 (m), 155 (m), 117 (m)

Table IV.4: Raman data of modified Co-molybdates obtained by the citrate method.

Composition	Raman shifts (cm^{-1})
Co-La-Mo	929* (vs), 913 (s), 886.5 (w), 876 (w), 811 (s), 712 (w), 674 (w), 467 (w), 362.3 (w), 348 (w), 326 (m), 311 (w)
Co-Ce-Mo	929* (vs), 908 (s), 882 (s), 811 (s), 768 (w), 740.8 (w), 365 (s), 324.6 (s), 305 (w)
Co-Pr-Mo	941-932 (vs), 911 (s), 877 (m), 857 (m), 814 (s), 767 (w), 737 (w), 363.5 (m), 326 (m)
Co-Sm-Mo	929* (vs), 904-889 (vs), 865 (w), 808 (s), 752 (w), 385 (w), 365 (w), 330 (m), 311 (w), 279 (w)
Co-Tb-Mo	946-936 (v), 911 (w), 897 (m), 877 (w), 850 (m), 816 (s), 741 (w), 362 (m), 353 (w), 327 (s), 298 (w), 280 (w)
Co-Bi-Mo	955 (w), 934 (vs), 923.2 (w), 899 (vs), 852 (m), 841 (w), 811 (s), 653 (m), 501 (w), 364 (s), 330 (m), 259 (w), 188 (s), 175 (w), 139 (m), 116 (w)

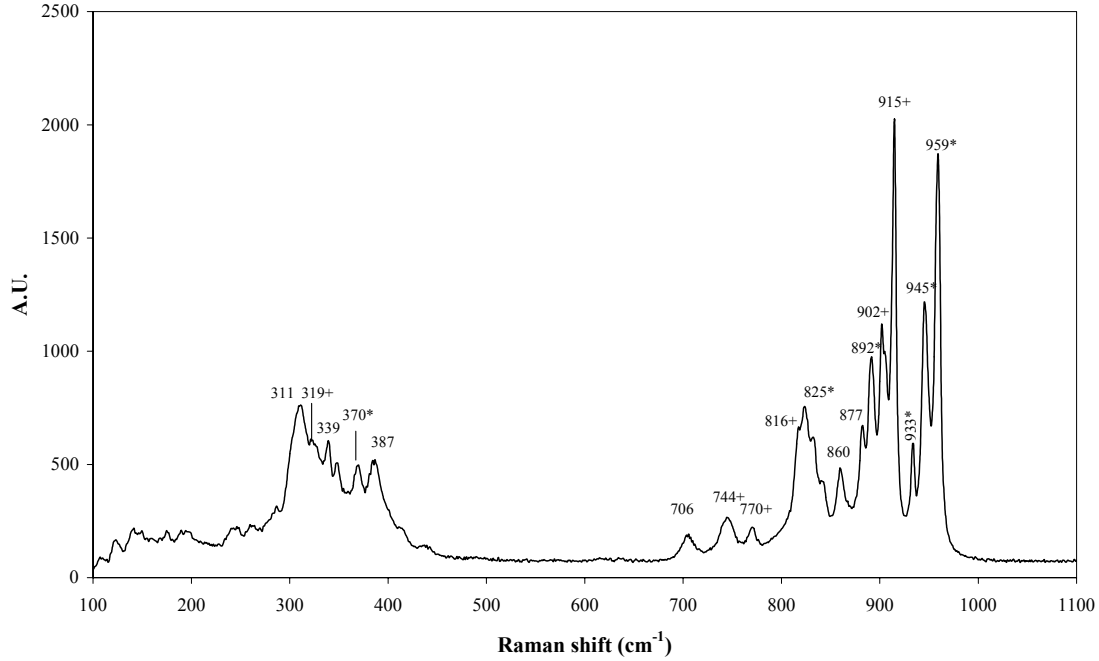

Fig.IV.2: Raman spectrum of Ni-Pr-Mo prepared by the citrate method: (*,+) main lines of β-$NiMoO_4$ and $Pr_2Mo_3O_{12}$, respectively.

IV.1.4 UV-visible diffuse reflectance spectroscopy

All modified catalysts as well the pure bulk phases have been analyzed by UV-visible DRS. The DR spectrum of $Bi_2Mo_3O_{12}$ exhibits the charge transfer (CT) band $O^{2-} \rightarrow Mo^{6+}$ below 440 nm and assigned to [MoO_4] species (111). In the Ni-Bi-Mo sample, this CT band overlaps another CT band due to the charge transfer $O^{2-} \rightarrow Mo^{6+}$ related to Ni-molybdate below 470 nm. In the Co-Bi-Mo-sample, the CT band of $Bi_2Mo_3O_{12}$ below 440 nm is also not visible because of the overlap with the CT band of the α-phase starting at 480 nm.

In pure $Pr_2Mo_3O_{12}$ (fig. IV.3), several sharp absorption bands are observed at 450, 475, 480 and 595 nm, which are assigned to ligand-field essentially independent f-f transitions of Pr^{3+} ions with $4f^2$ electron configuration, under conditions of extensive spin-orbit coupling. These bands are very similar to those observed in aqueous solutions of Pr(III) nitrate (445, 468, 482 and 589 nm). According to the literature (174), the bands observed here in the wavenumber range 16800-22000 cm^{-1} correspond to electronic transitions between the $^3H_4$ ground level to the following excited states: $^1D_2$ (595 nm), $^3P_0$ (480 nm), $^3P_1$ (475 nm) and $^3P_2$ (450 nm). The shoulder visible at about 465 nm corresponds to the $^3H_4 \rightarrow {}^1I_6$ transitions. The Ni-Pr-Mo sample (fig. IV.4) shows the major absorption bands of $Pr_2Mo_3O_{12}$ and also the CT band below 470 nm

characteristic of the distorted octahedral Mo coordination. The Co-Pr-Mo sample shows the absorption bands of $Pr_2Mo_3O_{12}$ but only between 500 and 425 nm, because those between 625 and 575 nm overlap the absorption band of $[CoO_6]$ octahedral (111).

The pure phase $La_2Mo_3O_{12}$ is characterized by a band starting at 370 nm. But in the case of Ni-La-Mo and Co-La-Mo catalysts, this band is masked by the CT band $O^{2-} \rightarrow Mo^{6+}$ starting at 480 nm and characteristic of α-$NiMoO_4$.

The pure $Sm_2Mo_3O_{12}$ phase sharp different absorption bands at 364, 378, 392, 406, 420, 439, 452, 464, 482, 500, 530 and 561 nm, assigned to f-f transitions of the $4f^5$ Sm^{3+} ion. In the Ni-Sm-Mo sample, six of these bands have been detected at 406, 420, 439, 464, 482, 530 and 561 nm, besides the usual CT band starting at 480 nm. In the case of Co-Sm-Mo sample, two weak peaks characteristic of this Sm-Mo-O phase are identified (at 406 and 463 nm), the others being overlapped by the absorption band of $[CoO_6]$ octahedra.

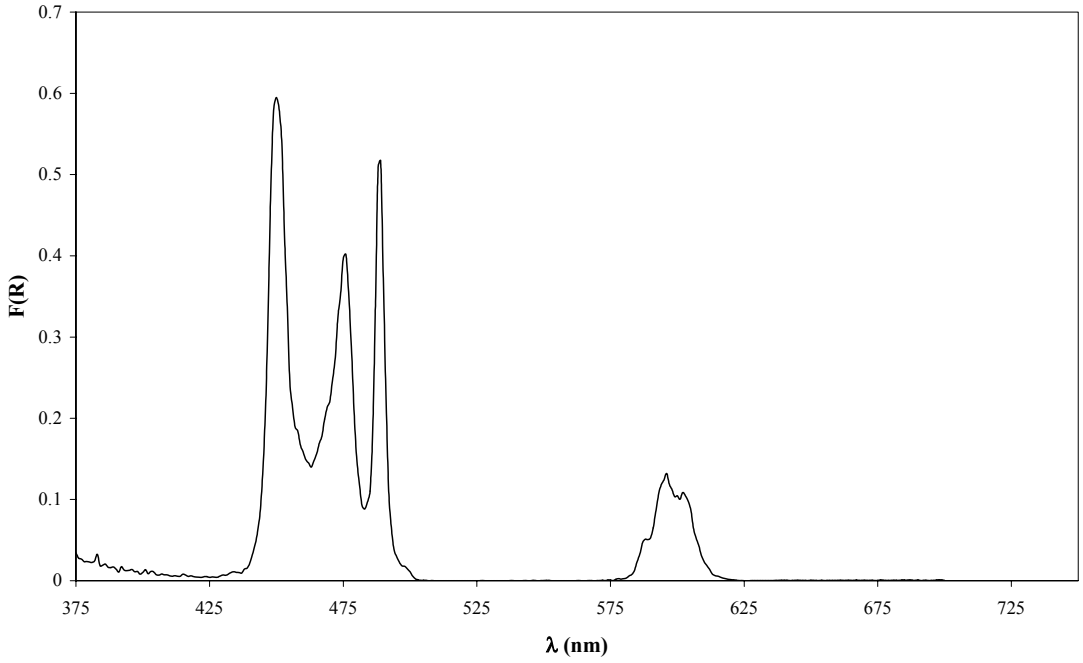

Fig.IV.3: UV-Vis diffuse reflectance spectrum of $Pr_2Mo_3O_{12}$ prepared by the citrate method.

In the catalysts modified by Ce or Tb, the spectra show the bands characteristic of Ni/Co molybdates, but no peaks that would indicate the presence of $Ce_2Mo_3O_{12}$ or $Tb_2Mo_3O_{12}$ are detected.

The overall picture of the citrate-prepared catalysts resulting from the use of all these techniques is an intimate mixture of two different quaternary phases, one based on

$MMoO_4$ and another based on $Ln_2Mo_3O_{12}$, both phases being possibly modified by incorporating foreign ions from the other one.

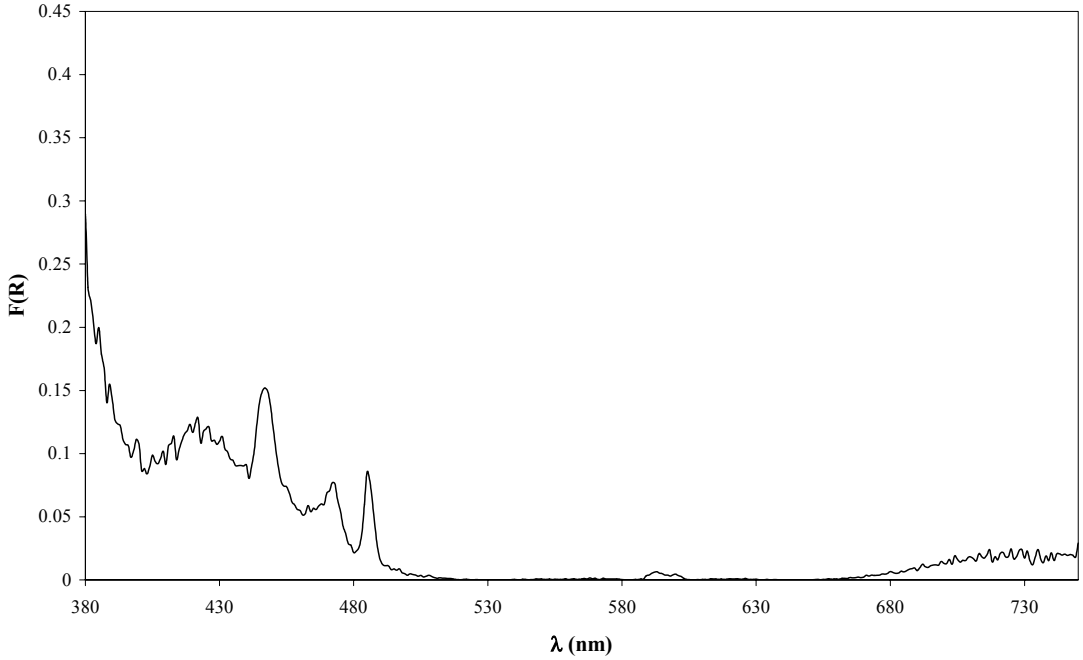

Fig.IV.4: UV-Vis diffuse reflectance spectrum of Ni-Pr-Mo (1:1:2.5) sample prepared by the citrate method.

IV.2 Characterization of M-Ln(Bi)-Mo-Si (1:1:2.5:20) prepared by the sol-gel method

IV.2.1 Thermal behaviour

Figure IV.5 displays the thermograms of Ni-La-Mo-Si and Ni-Ce-Mo-Si compounds as exemples. In sol-gel-prepared catalysts two different types of thermal degradation schemes are observed. Almost all thermograms are characterized by a progressive weight loss between 573 and 1073 K. Only the TGA of M-Ce-Mo (M = Ni or Co) samples exhibit an abrupt degradation between 1023 and 1123 K. In consequence to these results, two different calcinations conditions have been used for the sol-gel-prepared catalysts: 773 K / 20h and 1073 K / 10 h in a flow of 1 $l \cdot min^{-1}$ of dry air

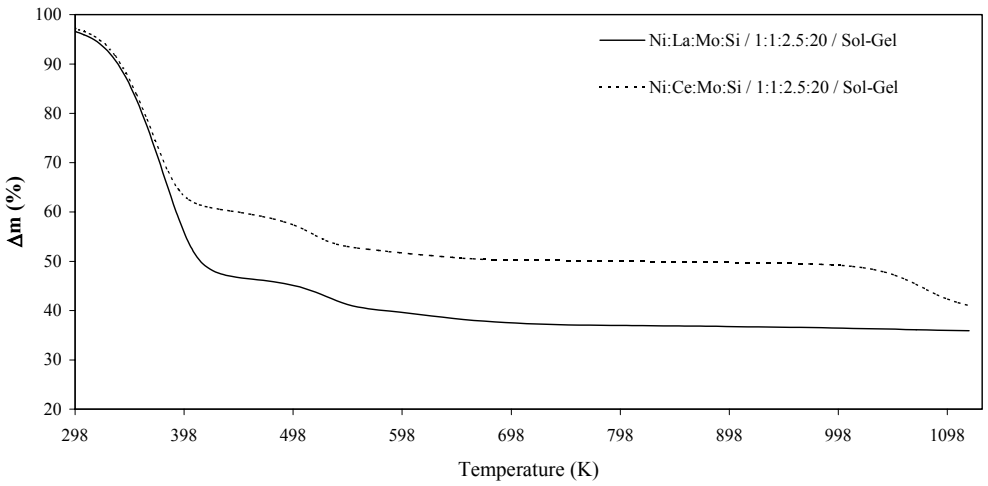

Fig.IV.5: Thermograms of Ni-La-Mo-Si and Ni-Bi-Mo-Si samples.

IV.2.2 X-ray diffraction and BET specific surface areas

Table IV.5: Composition, specific surface area and crystalline phases detected in modified Ni or Co molybdates prepared by the sol-gel method.

Composition	Temperature (K)	S_{BET} (m^2g^{-1})	Detected crystalline phases (XRD)
Ni-La-Mo-Si	773	275	β-$NiMoO_4$*
	1073	49	β-$NiMoO_4$*
Ni-Ce-Mo-Si	773	378	β-$NiMoO_4$* + MoO_3 + CeO_2
	1073	106	β-$NiMoO_4$* + CeO_2*
Ni-Pr-Mo-Si	773	303	MoO_3
	1073	20	β-$NiMoO_4$*
Ni-Sm-Mo-Si	773	272	β-$NiMoO_4$*
	1073	56	β-$NiMoO_4$*
Ni-Tb-Mo-Si	1073	39	β-$NiMoO_4$*
Ni-Bi-Mo-Si	773	83	β-$NiMoO_4$* + $Bi_2Mo_3O_{12}$*
	1073	8	β-$NiMoO_4$* + $Bi_2Mo_2O_9$*
Co-La-Mo-Si	773	321	β-$CoMoO_4$* + MoO_3
	1073	22	β-$CoMoO_4$*
Co-Ce-Mo-Si	773	310	β-$CoMoO_4$* + MoO_3 + CeO_2
	1073	30	β-$CoMoO_4$* + CeO_2*
Co-Pr-Mo-Si	773	291	β-$CoMoO_4$* + MoO_3
	1073	20	β-$CoMoO_4$*
Co-Sm-Mo-Si	773	294	β-$CoMoO_4$* + MoO_3
	1073	43	β-$CoMoO_4$* + Sm_2O_3
Co-Tb-Mo-Si	1073	21	β-$CoMoO_4$*
Co-Bi-Mo-Si	773	254	β-$CoMoO_4$* + $Bi_2Mo_3O_{12}$*
	1073	6.6	β-$CoMoO_4$* + $Bi_2Mo_2O_9$*

* = the experimental diffraction lines are slightly shifted with respect to those of the reference phases

IV.2.3 X-ray photoelectron spectroscopy

Table IV.6: Relative atomic intensity ratios measured by XPS in modified Ni or Co molybdates prepared by sol-gel method (calcination at 773 K).

M = Ni, Co M' = La, Ce, Pr, Sm, Bi	M/Mo		M'/Mo		M/M'		M/Si		M'/Si		Mo/Si	
	Exp	Th	Exp	Th	Exp	Th	Exp	Th	Exp	Th	Exp	Th
Ni-La-Mo-Si	0.098	0.4	0.19	0.4	0.51	1	0.012	0.05	0.024	0.05	0.123	0.125
Ni-Ce-Mo-Si	0.175	0.4	0.14	0.4	1.23	1	0.0066	0.05	0.0053	0.05	0.037	0.125
Ni-Pr-Mo-Si	0.25	0.4	0.56	0.4	0.45	1	0.0082	0.05	0.018	0.05	0.033	0.125
Ni-Sm-Mo-Si	0.27	0.4	0.09	0.4	3	1	0.035	0.05	0.012	0.05	0.132	0.125
Ni-Bi-Mo-Si	0.12	0.4	0.27	0.4	0.43	1	0.012	0.05	0.028	0.05	0.105	0.125
Co-La-Mo-Si	0.40	0.4	0.53	0.4	0.4	1	0.0067	0.05	0.017	0.05	0.031	0.125
Co-Ce-Mo-Si	0.07	0.4	0.098	0.4	0.75	1	0.0038	0.05	0.005	0.05	0.051	0.125
Co-Pr-Mo-Si	0.14	0.4	0.4	0.4	0.33	1	0.0057	0.05	0.017	0.05	0.041	0.125
Co-Sm-Mo-Si	0.25	0.4	0.11	0.4	2.23	1	0.024	0.05	0.011	0.05	0.096	0.125
Co-Bi-Mo-Si	0.12	0.4	0.21	0.4	0.58	1	0.011	0.05	0.019	0.05	0.088	0.125

The binding energies of the various elements involved in catalyst formulation were found in the following ranges: 856.0 ± 0.3 eV for Ni $2p_{3/2}$, 781.3 ± 0.3 eV for Co $2p_{3/2}$, 232.7 ± 0.3 eV for Mo $3d_{5/2}$, 159.8 ± 0.2 eV for Bi $4f_{7/2}$, 835.6 ± 0.1 eV for La $3d_{5/2}$, 934.3 ± 0.1 eV for Pr $3d_{5/2}$, 900.6 ± 0.4 eV for Ce $3d_{3/2}$, 1083.5 ± 0.2 eV for Sm $3d_{5/2}$, 103.7 ± 0.3 eV for Si 2p. In all samples, the elements are characterized by their normally expected oxidation states: Ni(II), Co(II), Mo(VI), Ln(III), Ce(IV), Bi(III).

Table IV.7: Relative atomic intensity ratios measured by XPS in modified Ni or Co molybdates prepared by sol-gel method (calcination at 1073 K).

M = Ni, Co M' = La, Ce, Pr, Sm, Bi	M/Mo		M'/Mo		M/M'		M/Si		M'/Si		Mo/Si	
	Exp	Th	Exp	Th	Exp	Th	Exp	Th	Exp	Th	Exp	Th
Ni-La-Mo-Si	0.11	0.4	0.27	0.4	0.42	1	0.0056	0.05	0.013	0.05	0.050	0.125
Ni-Ce-Mo-Si	0.10	0.4	0.20	0.4	0.45	1	0.0045	0.05	0.0098	0.05	0.045	0.125
Ni-Pr-Mo-Si	0.085	0.4	0.17	0.4	0.50	1	0.0064	0.05	0.013	0.05	0.075	0.125
Ni-Sm-Mo-Si	0.18	0.4	0.25	0.4	0.73	1	0.01	0.05	0.014	0.05	0.056	0.125
Ni-Bi-Mo-Si	0.19	0.4	0.46	0.4	0.42	1	0.012	0.05	0.028	0.05	0.061	0.125
Co-La-Mo-Si	0.18	0.4	0.35	0.4	0.51	1	0.0059	0.05	0.012	0.05	0.033	0.125
Co-Ce-Mo-Si	0.11	0.4	0.16	0.4	0.72	1	0.0064	0.05	0.0087	0.05	0.056	0.125
Co-Pr-Mo-Si	0.093	0.4	0.20	0.4	0.46	1	0.0038	0.05	0.0083	0.05	0.041	0.125
Co-Sm-Mo-Si	0.2	0.4	0.21	0.4	0.98	1	0.014	0.05	0.015	0.05	0.068	0.125
Co-Bi-Mo-Si	0.16	0.4	0.45	0.4	0.35	1	0.01	0.05	0.03	0.05	0.065	0.125

IV.2.4 Raman spectroscopy

Table IV.8: Raman data of modified Ni or Co molybdates obtained by the sol-gel method (calcined at 1073 K).

Composition	Raman shifts (cm^{-1})
Ni-La-Mo-Si	959-946 (vs), 926 (w), 913 (m), 902 (m), 892 (m), 860 (w), 853 (w), 841 (w), 826 (m), 389 (m), 372 (m), 349 (w), 341 (w), 314 (w), 300 (w)
Ni-Ce-Mo-Si	957-944 (vs), 911 (w), 889 (m), 858 (m), 852 (w), 825 (m), 460 (vs), 388 (m), 374 (m), 348 (w), 348 (w), 339 (m)
Ni-Pr-Mo-Si	959(vs), 911 (m), 704 (m), 384 (w), 371 (w)
Ni-Sm-Mo-Si	960-946 (vs), 913 (w), 903-894 (vs), 872 (w), 846 (m), 826 (s), 749 (w), 705 (w), 489 (w), 442 (w), 389 (m), 372 (m), 349 (w), 341 (m), 325 (w), 304 (w), 290 (w)
Ni-Tb-Mo-Si	958-946 (vs), 914 (w), 902-892 (s), 824 (s), 438 (w), 389 (m), 370 (m), 348 (w), 340 (w), 329 (w)
Ni-Bi-Mo-Si	961-946 (vs), 913-902 (s), 885 (vs), 827 (m), 757 (m), 705 (m), 386 (w), 369 (w), 360 (w), 340 (w), 327 (w), 283 (m)
Co-La-Mo-Si	944-935 (vs), 911 (m), 841 (w), 814 (m), 365.7 (m), 338 (w), 328 (m)
Co-Ce-Mo-Si	943-934 (vs), 913 (w), 876 (w), 856 (m), 814 (s), 458 (w), 365.2 (m), 352 (w), 325.7(m)
Co-Pr-Mo-Si	943-935(vs), 877 (w), 838 (w), 814 (m), 364 (m), 322 (m)
Co-Sm-Mo-Si	948-937 (vs), 877 (w), 814 (s), 698 (w), 367 (w), 349 (w), 337 (w), 327 (w), 299 (w), 283 (w)
Co-Tb-Mo-Si	959-947 (vs), 939 (s), 901-892 (s), 825 (s), 388 (m), 369 (m), 349 (w), 341 (w), 328 (w), 298 (w), 289 (w)
Co-Bi-Mo-Si	947-936 (vs), 885 (vs), 816 (s), 758 (m), 365 (m), 337 (w), 329 (w), 283 (w)

IV.3 Characterization of Ni-Co-Ln(Bi)-Mo-Si (1:1:1:2.5:20) and Ni-Co-Ln-Ln'(Bi)-Mo-Si (1:1:1:1:2.5:20) prepared by the sol-gel method

IV.3.1 Thermal behaviour

Figure IV.6 displays the thermograms of Ni-Co-La-Mo-Si, Ni-Co-Ce-Mo-Si (1:1:1:2.5:20) and Ni-Co-La-Ce-Mo-Si (1:1:1:1:2.5:20) samples. In all cases we observed the same thermal degradation scheme. In consequence to these results, the calcination conditions adopted for the modified mixed nickel and cobalt molybdates prepared by sol-gel method were fixed at 773 K in a flow of 1 $l \cdot min^{-1}$ of dry air for 20 h.

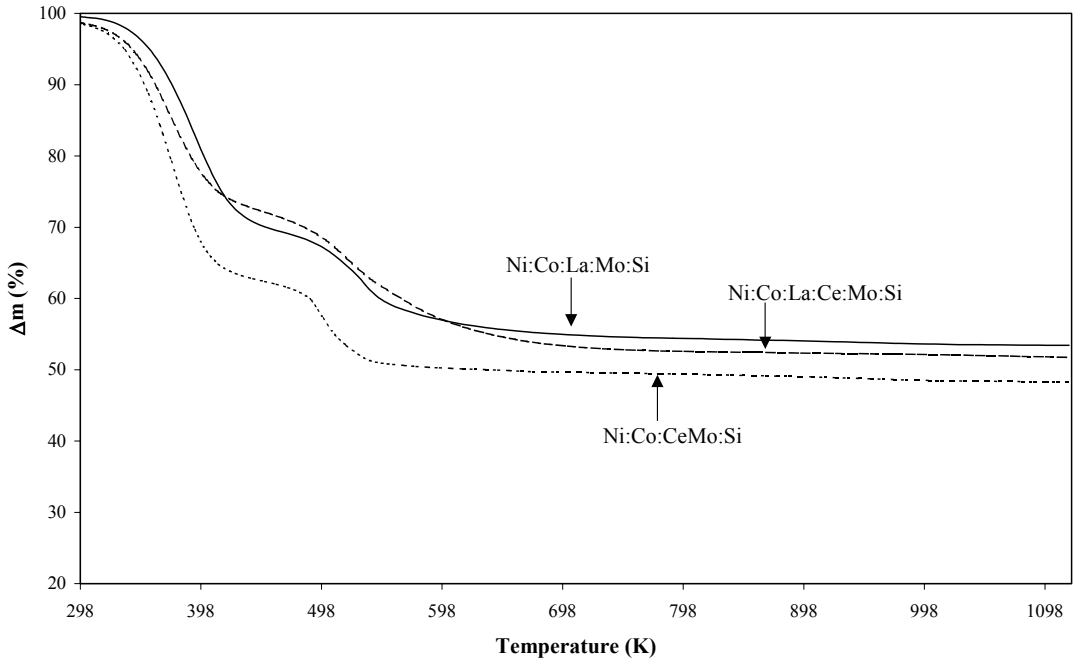

Fig.IV.6: Thermograms of Ni-Co-La-Mo-Si, Ni-Co-Ce-Mo-Si (1:1:1:2.5:20) and Ni-Co-La-Ce-Mo-Si (1:1:1:1:2.5:20), prepared by the sol-gel method.

IV.3.2 X-ray diffraction and BET specific surface areas

Table IV.9: Composition, specific surface area and crystalline phases detected in Ni-Co-Ln(Bi)-Mo-Si catalysts prepared by the sol-gel method

Composition and molar ratio	S_{BET} (m^2 g^{-1})	Detected crystalline phases (XRD)
Ni:Co:Mo:Si 1 :1 :2.5 :20	279	β-$Ni_{1-x}Co_xMoO_4$
Ni :Co :La :Mo :Si 1 :1 :1 :2.5 :20	301	β-$Ni_{1-x}Co_xMoO_4$
Ni :Co :Ce :Mo :Si 1 :1 :1 :2.5 :20	311	β-$Ni_{1-x}Co_xMoO_4$ + MoO_3 + CeO_2
Ni :Co :Pr :Mo :Si 1 :1 :1 :2.5 :20	293	β-$Ni_{1-x}Co_xMoO_4$
Ni :Co :Sm :Mo :Si 1 :1 :1 :2.5 :20	349	β-$Ni_{1-x}Co_xMoO_4$
Ni :Co :Tb :Mo :Si 1 :1 :1 :2.5 :20	318	β-$Ni_{1-x}Co_xMoO_4$
Ni :Co :Bi :Mo :Si 1 :1 :1 :2.5 :20	288	β-$Ni_{1-x}Co_xMoO_4$ + $Bi_2Mo_3O_{12}$
Ni :Co :La :Ce :Mo :Si 1 :1 :1 :1 :2.5 :20	337	β-$Ni_{1-x}Co_xMoO_4$
Ni :Co :La :Pr :Mo :Si 1 :1 :1 :1 :2.5 :20	272	β-$Ni_{1-x}Co_xMoO_4$
Ni :Co :Ce :Pr :Mo :Si 1 :1 :1 :1 :2.5 :20	325	β-$Ni_{1-x}Co_xMoO_4$
Ni :Co :La :Bi :Mo :Si 1 :1 :1 :1 :2.5 :20	277	β-$Ni_{1-x}Co_xMoO_4$
Ni :Co :Pr :Bi :Mo :Si 1 :1 :1 :1 :2.5 :20	256	β-$Ni_{1-x}Co_xMoO_4$
Ni :Co :Ce :Bi :Mo :Si 1 :1 :1 :1 :2.5 :20	339	β-$Ni_{1-x}Co_xMoO_4$
Ni :Co :Sm :La :Mo :Si 1 :1 :1 :1 :2.5 :20	222	β-$Ni_{1-x}Co_xMoO_4$
Ni :Co :Sm :Pr :Mo :Si 1 :1 :1 :1 :2.5 :20	293	β-$Ni_{1-x}Co_xMoO_4$
Ni :Co :Sm :Ce :Mo :Si 1 :1 :1 :1 :2.5 :20	228	β-$Ni_{1-x}Co_xMoO_4$
Ni :Co :Sm :Bi :Mo :Si 1 :1 :1 :1 :2.5 :20	296	β-$Ni_{1-x}Co_xMoO_4$
Ni :Co :Tb :La :Mo :Si 1 :1 :1 :1 :2.5 :20	237	β-$Ni_{1-x}Co_xMoO_4$
Ni :Co :Tb :Pr :Mo :Si 1 :1 :1 :1 :2.5 :20	268	β-$Ni_{1-x}Co_xMoO_4$
Ni :Co :Tb :Ce :Mo :Si 1 :1 :1 :1 :2.5 :20	277	β-$Ni_{1-x}Co_xMoO_4$
Ni :Co :Tb :Sm :Mo :Si 1 :1 :1 :1 :2.5 :20	253	β-$Ni_{1-x}Co_xMoO_4$
Ni :Co :Tb :Bi :Mo :Si 1 :1 :1 :1 :2.5 :20	261	β-$Ni_{1-x}Co_xMoO_4$

IV.3.3 Raman and X-ray photoelectron spectroscopy

Ni-Co-Ln(Bi)-Tb-Mo-Si-catalysts were analyzed by Raman spectroscopy (see table IV.10) and the comparison with reference spectra generally confirms the presence of solid solutions of β-$NiMoO_4$ and β-$CoMoO_4$.

Table IV.10: Raman data of some modified mixed Ni and Co molybdates obtained by the sol-gel method.

Composition	Raman shifts (cm^{-1})
Ni-Co-La-Mo-Si	948-938 (vs), 881 (m), 817 (m), 376 (m), 333 (m), 287 (m), 238 (w)
Ni-Co-Ce-Mo-Si	931*(vs), 875 (m), 810 (m), 445 (m), 360 (w)
Ni-Co-Pr-Mo-Si	930*(vs), 876 (m), 810 (m), 354 (w), 332 (w)
Ni-Co-Tb-Mo-Si	930*(vs), 875 (m), 808 (m), 361 (w), 334 (w)
Ni-Co-Bi-Mo-Si	930* (vs), 873 (m) 806 (m), 360 (w)

* = with a shoulder

The XPS binding energies of the various elements present in the catalysts were found in the following ranges: 856.2 ± 0.3 eV for Ni $2p_{3/2}$, 781.2 ± 0.3 eV for Co $2p_{3/2}$, 232.7 ± 0.1 eV for Mo $3d_{5/2}$, 159.9 ± 0.1 eV for Bi $4f_{7/2}$, 835.4 ± 0.2 eV for La $3d_{5/2}$, 934.2 ± 0.1 eV for Pr $3d_{5/2}$, 900.1 ± 0.4 eV for Ce $3d_{3/2}$, 1083.9 ± 0.1 eV for Sm $3d_{5/2}$, 103.6 ± 0.1 eV for Si 2p. According to the XPS analysis, bismuth and all lanthanides but Ce are present in their trivalent state; cerium appears in its (+IV) oxidation state and the same is assumed for terbium.

Tables IV.11 and 12 summarize the XPS atomic intensity ratios of Ni:Co:Ln(Bi):Mo:Si (1:1:1:2.5:20) and Ni:Co:Ln:Ln':Mo:Si (1:1:1:1:2.5:20), respectively. The major trends with respect to the surface composition of these catalysts are described hereafter.

Ni:Co:Ln(Bi):Mo:Si (Table IV.11)

In La-, Ce-, Bi-based catalysts (Co/Ni)exp>(Co/Ni)th. Taking into account the (Ni,Co)/Si values, Ni and Co appear to be better dispersed in the Bi-modified catalyst. Ce- and Pr-modified catalysts are those characterized by the highest (Ni,Co/Mo) values, therefore their surface is enriched in Ni and Co. In Pr- and Sm-based catalysts, the high (Ln/Mo) values lead us to conclude that their surfaces are enriched in Pr and Sm and that Sm is the best-dispersed lanthanide (because of the highest experimental Sm/Si

ratio). In general Mo seems to be well dispersed on the surface of the catalysts (see Mo/Si ratios), particularly in the Bi-based one.

Table IV.11: XPS results of Ni:Co:Ln(Bi):Mo:Si (1:1:1:2.5:20) prepared by the sol-gel method and calcined at 773 K.

M=Ni,Co	**Ni/Mo Co/Mo**		**M'/Mo**		**Ni/M' Co/M'**		**Ni/Si Co/Si**		**M'/Si**		**Mo/Si**		**Co/Ni**	
M' = La,Ce,Pr,Sm,Bi	**Exp.**	**Th.**	**Exp.**	**Th.**	**Exp.**	**Th.**	**Exp.**	**Th.**	**Exp.**	**Th.**	**Exp.**	**Th.**	**Exp.**	**Th.**
Ni : Co : La : Mo: Si	0.065	0.4	0.15	0.4	0.43	1	0.008	0.05	0.019	0.05	0.126	0.125	2.08	1
1 : 1 : 1 : 2.5 : 20	0.134	0.4			0.89	1	0.017	0.05						
Ni : Co : Ce : Mo: Si	0.18	0.4	0.07	0.4	2.46	1	0.012	0.05	0.005	0.05	0.067	0.125	1.05	1
1 : 1 : 1 : 2.5 : 20	0.19	0.4			2.6	1	0.013	0.05						
Ni : Co : Pr : Mo : Si	0.22	0.4	0.23	0.4	1	1	0.016	0.05	0.016	0.05	0.07	0.125	0.66	1
1 : 1 : 1 : 2.5 : 20	0.15	0.4			0.66	1	0.011	0.05						
Ni : Co : Sm : M : Si	0.086	0.4	0.213	0.4	0.40	1	0.009	0.05	0.023	0.05	0.109	0.125	0.67	1
1 : 1 : 1 : 2.5 : 20	0.057	0.4			0.27	1	0.006	0.05						
Ni : Co : Bi : Mo : Si	0.12	0.4	0.05	0.4	2.6	1	0.023	0.05	0.009	0.05	0.2	0.125	1.15	1
1 : 1 : 1 : 2.5 : 20	0.13	0.4			2.3	1	0.027	0.05						

Ni-Co-Ln-Ln'(Bi)-Mo-Si (Table IV.12)

The experimental atomic (Co/Ni) ratios are higher than the corresponding theoretical ones: Co is definitely better detected than Ni in all catalysts. Moreover, because the experimental atomic (Ni,Co/M,M') or (Ni,Co/Si) ratios are higher or very close to the theoretical ones and that the experimental (M,M'/Si) ratios are lower than the corresponding theoretical ones, it can be assumed that Ni and Co are better detected on the surface of the samples than the lanthanides or bismuth. It could be noticed that (Mo/Si)exp>(Mo/Si)th in all cases except in those catalysts in which Bi is involved in the formulation. On the basis of the (M/M') ratios, Sm appears to be the element which is the most difficult to detect.

Table IV.12: XPS results of Ni:Co:M:M':Mo:Si (1:1:1:1:2.5:20) samples prepared by the sol-gel method and calcined at 773 K. (Fresh catalysts)

Ni:Co:M:M':Mo:Si 1 : 1 : 1 : 1 : 2.5 : 20	Ni/Mo Co/Mo		M/Mo M'/Mo		Ni/M Co/M		Ni/M' Co/M'		Ni/Si Co/Si		M/Si M'/Si		Mo/Si		Co/Ni		M/M'	
	Exp.	**Th.**	**Exp.**	**Th.**	**Exp.**	**Th.**	**Exp.**	**Th.**	**Exp.**	**Th.**	**Exp.**	**Th.**	**Exp.**	**Th.**	**Exp.**	**Th.**	**Exp.**	**Th.**
M = La M' = Ce	0.13 0.18	0.4 0.4	0.07 0.03	0.4 0.4	1.72 2.5	1 1	3.9 5.6	1 1	0.04 0.06	0.05 0.05	0.024 0.011	0.05 0.05	0.33	0.125	1.45	1	2.25	1
M = La M' = Pr	0.105 0.14	0.4 0.4	0.07 0.05	0.4 0.4	1.5 2.04	1 1	2.13 2.9	1 1	0.038 0.05	0.05 0.0(5	0.025 0.018	0.05 0.05	0.36	0.125	1.35	1	1.4	1
M = Ce M' = Pr	0.11 0.16	0.4 0.4	0.05 0.07	0.4 0.4	2.18 3.18	1 1	1.55 2.27	1 1	0.047 0.068	0.05 0.05	0.021 0.030	0.05 0.05	0.43	0.125	1.46	1	0.71	1
M = La M' = Bi	0.089 0.136	0.4 0.4	0.1 0.1	0.4 0.4	0.9 1.4	1 1	0.8 1.2	1 1	0.013 0.02	0.05 0.05	0.015 0.017	0.05 0.05	0.15	0.125	1.53	1	0.9	1
M = Pr M' = Bi	0.14 0.145	0.4 0.4	0.12 0.14	0.4 0.4	1.1 1.2	1 1	1 1.03	1 1	0.011 0.012	0.05 0.05	0.01 0.011	0.05 0.05	0.08	0.125	1.03	1	0.9	1
M = Ce M' = Bi	0.11 0.15	0.4 0.4	0.13 0.19	0.4 0.4	0.89 1.17	1 1	0.6 0.8	1 1	0.012 0.016	0.05 0.05	0.014 0.020	0.05 0.05	0.104	0.125	1.32	1	0.67	1
M = Sm M' = La	0.1 0.15	0.4 0.4	0.04 0.07	0.4 0.4	2.38 3.56	1 1	1.45 2.16	1 1	0.04 0.06	0.05 0.05	0.016 0.027	0.05 0.05	0.38	0.125	1.5	1	0.61	1
M = Sm M' = Pr	0.11 0.145	0.4 0.4	0.05 0.07	0.4 0.4	2.3 3.06	1 1	1.55 2.06	1 1	0.038 0.05	0.05 0.05	0.016 0.024	0.05 0.05	0.35	0.125	1.32	1	0.67	1
M = Sm M' = Ce	0.1 0.13	0.4 0.4	0.04 0.07	0.4 0.4	2.42 3.16	1 1	1.41 1.84	1 1	0.039 0.051	0.05 0.05	0.016 0.028	0.05 0.05	0.40	0.125	1.31	1	0.58	1

It has been shown in the literature (175,176), that upon exposure to atmospheric H_2O and CO_2, lanthana is partly transformed into a hydroxocarbonate. The final lanthanum oxide stabilized in air consists of a nucleus of crystalline $La(OH)_3$ surrounded by this hydroxocarbonate phase. In both Ni-Co-Ln-Mo-Si and Ni-Co-Ln-Ln'-Mo-Si samples, the presence of carbonates was detected by means of XPS. In all these catalysts, besides the components of the C1s peak at 284.8 and 286.6 eV assigned to C-(C,H) and C-O, respectively, a third peak lying in the range 288.3 – 288.5 eV is present, that may be assigned to surface carbonate species. In the same way, for all these samples, the O1s signals are fitted with two peaks at 530.9 ± 0.1 (O(I)) and 532.9 ± 0.1 (O(II)) (see fig. IV.7 and 8).

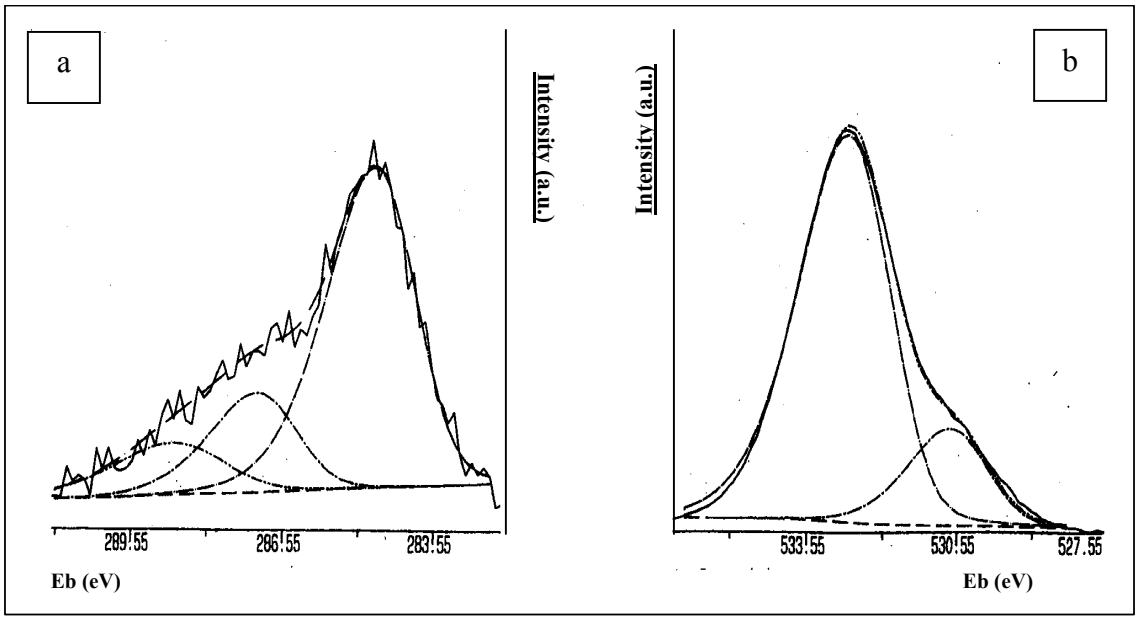

Fig.IV.7: (a) C1s and (b) O1s XPS spectrum of Ni-Co-La-Mo-Si.

In accordance with several earlier studies (177-179), the oxygen peak at the lower binding energy is attributed to lattice oxygen. Some authors (180) attributed the broad peak at higher binding energy to adsorbed oxygen or hydroxyl groups. However, as already stated, the presence of a third component at 288.3 eV in our C1s spectra led us to interpret the O(II) component by the presence of both hydroxyl and carbonate groups chemisorbed on the oxide. Table IV.13 lists the C1s/($La3d_{5/2}$+$Ce3d_{3/2}$) and O(II)/O(I) ratios of some samples in order to prove that when the (C/La+Ce) ratio increases, the O(II)/O(I) ratio follows the same evolution. In this case (as well as in all

other modified catalysts), (C/La+Ce) in Ni:Co:La:Ce:Mo:Si, is lower than (C/La) or (C/Ce) in Ni:Co:La(Ce):Mo:Si: in the latter case O(II)/O(I) is higher.

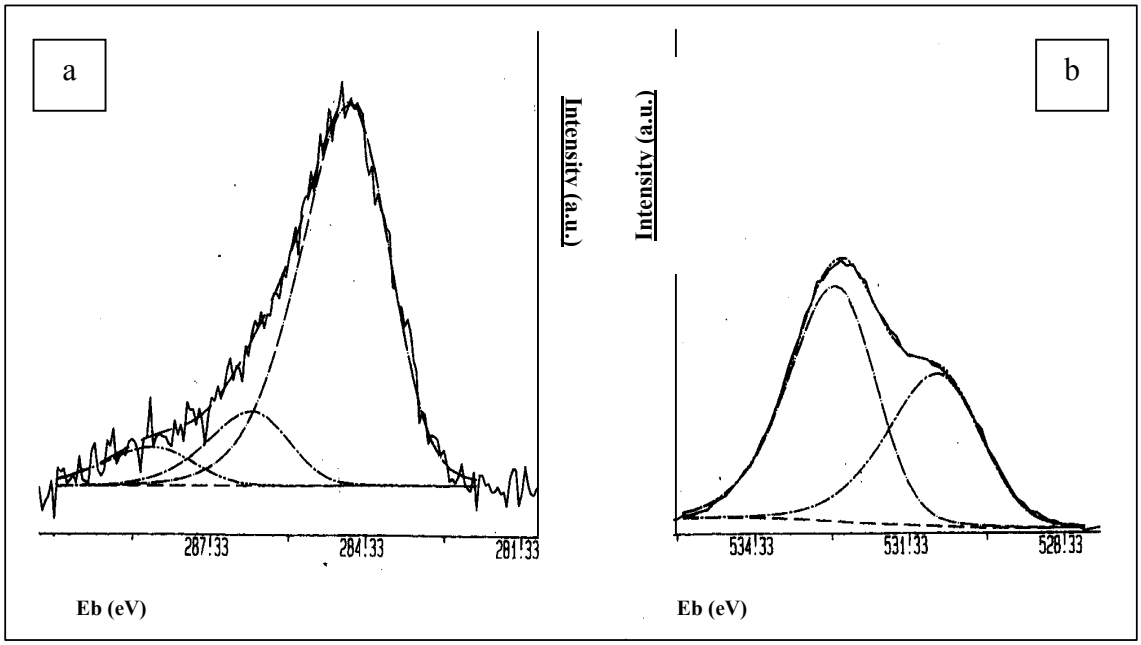

Fig.IV.8: (a) C1s and (b) O1s XPS spectrum of Ni-Co-La-Ce-Mo-Si.

Generally speaking, where the C content is higher, the possibility of forming carbonates increases. Moreover, in the case of La-modified catalysts, the binding energy value of $La3d_{5/2}$ has been found at 835.4 ± 0.2 eV. Galtayries et al. (178), reported for a La_2O_3 sample aged in air a binding energy value of $La3d_{5/2}$ equal to 835.1 eV: this value has been also found in an old lanthanum carbonate sample (177). This is a further assessment of the formation of carbonates on the surface of these modified catalysts.

Table IV.13: Experimental C1s/($La3d_{5/2}$+$Ce3d_{3/2}$), O(II)/O(I), C1s/$La3d_{5/2}$ and C1s/$Ce3d_{3/2}$ ratios in Ni :Co :La :Ce :Mo :Si and Ni :Co :La(Ce) :Mo :Si catalysts.

Additional elements	C1s/($La3d_{5/2}$+$Ce3d_{3/2}$)	C1s/$La3d_{5/2}$	C1s/$Ce3d_{3/2}$	O(II)/O(I)
La-Ce (fresh)	8.95			1.45
La (fresh)		10.48		4.56
Ce (fresh)			33.93	4.75
La-Ce (used)	9.95			2.12

IV.4 Catalytic Results

IV.4.1 Catalytic performances of "stoichiometric" M-Ln(Bi)-Mo-Si (M= Ni, Co) (1:1:2.5:20)

Adding a lanthanide or bismuth to a Ni-Mo based catalyst has a pronounced detrimental effect on the production of propene (fig.IV.9), which is totally inhibited; the higher propane conversion displayed by Pr- and Bi-modified catalysts ($XC_3° = 7.5$ and 4.5% at 753 K, respectively) is associated with a higher production of CO_2. The Pr-modified catalyst gives the highest oxygen conversion (at 753 K) together with Ce-, Sm- and Bi-modified catalysts (fig.IV.10); the Tb-modified one is not active at all.

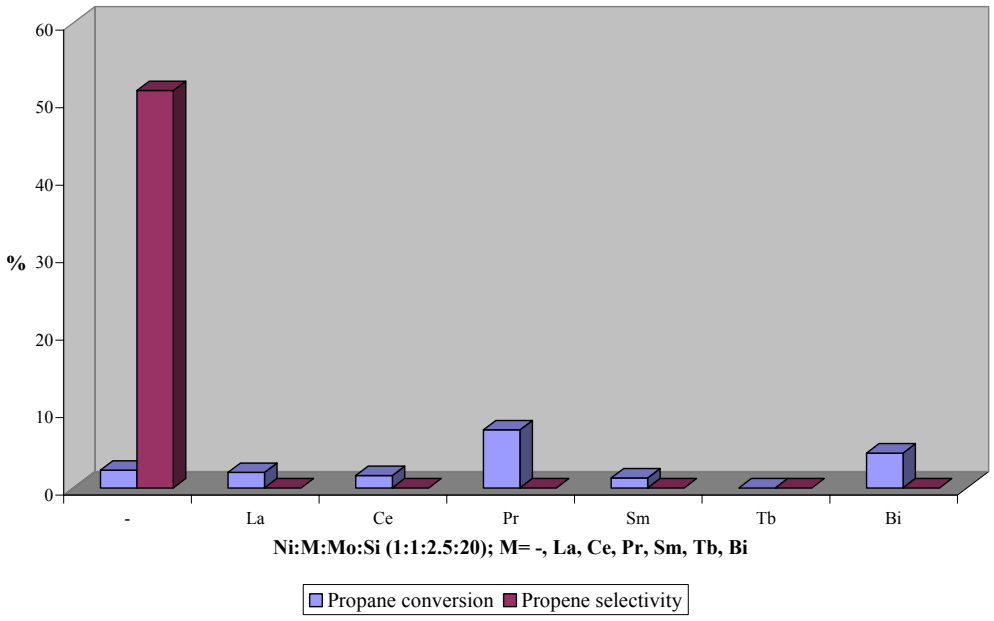

Fig.IV.9: Propane conversion and propene selectivity of Ni-M-Mo-Si (1:1:2.5:20) catalysts, at 753 K.

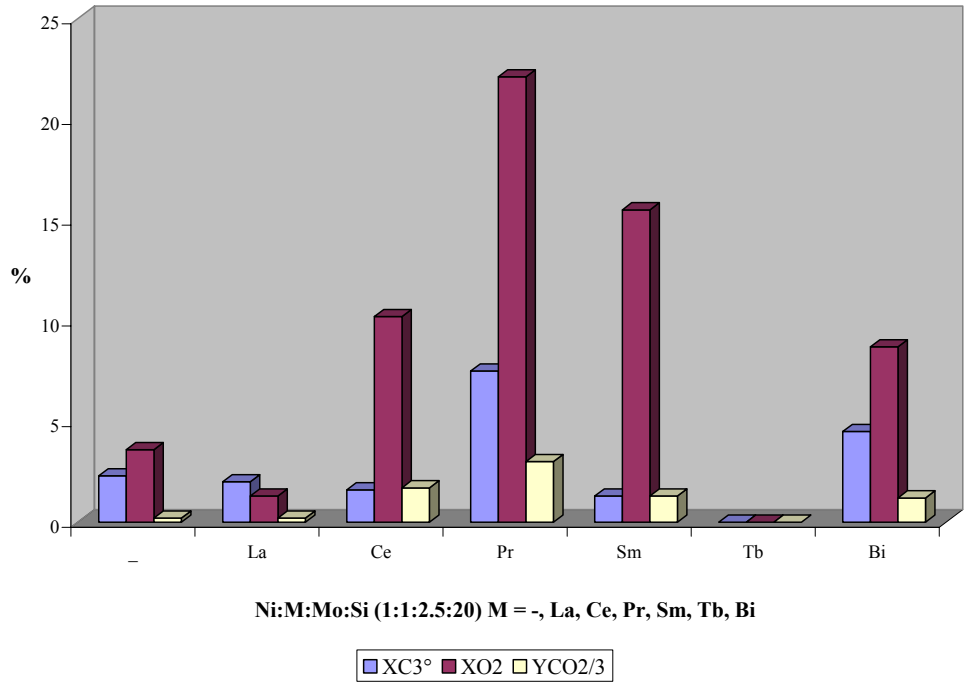

Fig.IV.10: Propane conversion ($XC_3°$), oxygen conversion (XO_2) and CO_2 yield ($YCO_2/3$) of Ni-M-Mo-Si (1:1:2.5:20) catalysts, at 753 K.

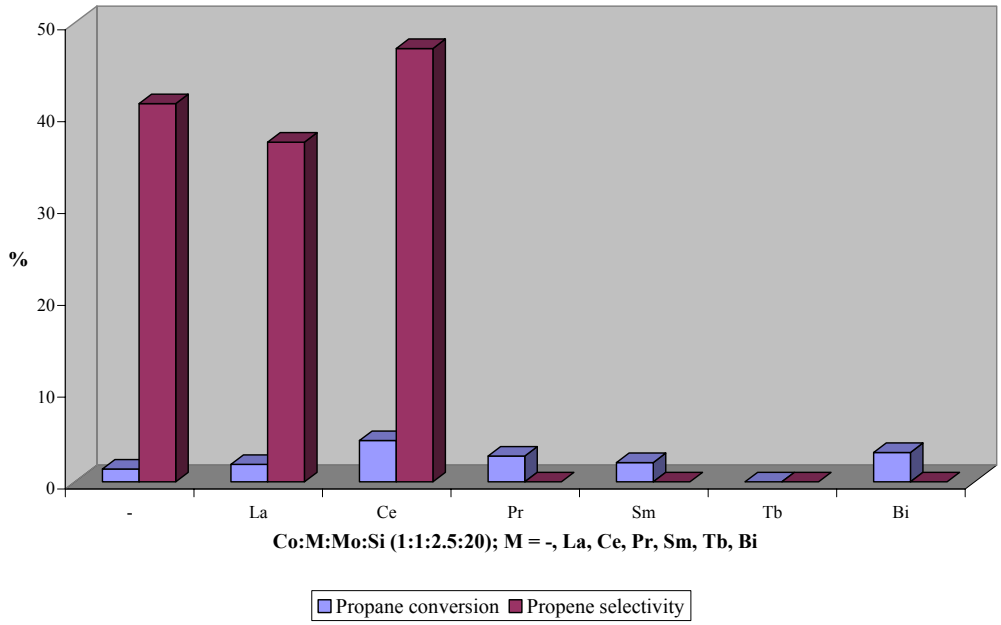

Fig.IV.11: Propane conversion and propene selectivity of Co-M-Mo-Si (1:1:2.5:20) catalysts, at 753 K.

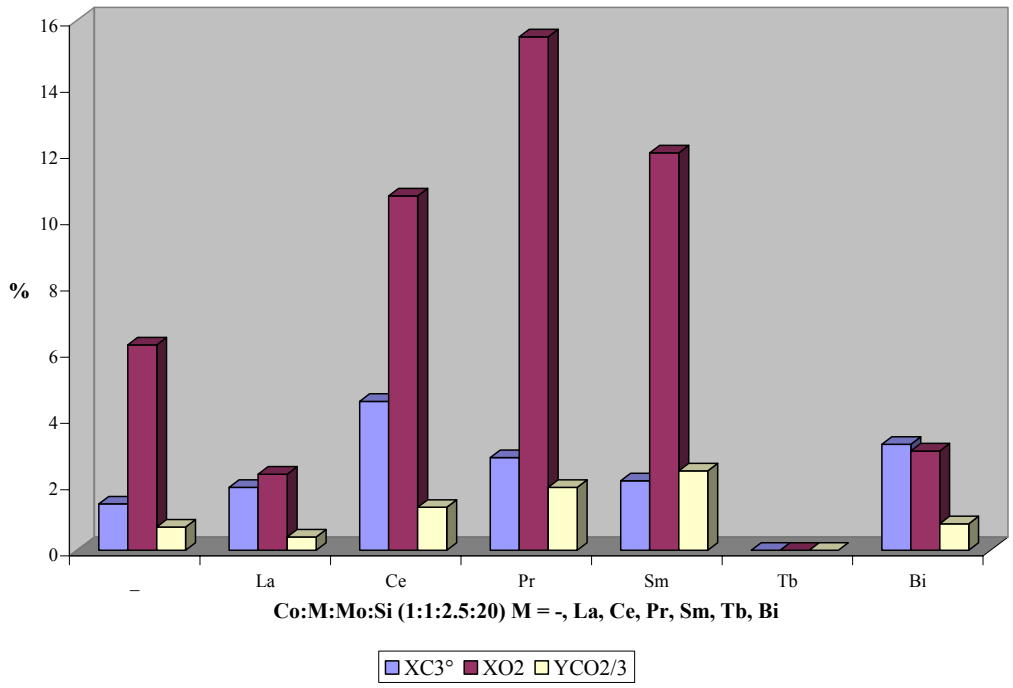

Fig.IV.12: Propane conversion ($XC_3°$), oxygen conversion (XO_2) and CO_2 yield ($YCO_2/3$) of Co-M-Mo-Si (1:1:2.5:20) catalysts, at 753 K.

In the Co-Mo-based catalysts (fig.IV.11), an enhancement of propane conversion and propene selectivity with respect to simple $CoMoO_4$ ($XC_3° = 1.4\%$, $SC_3^{=} = 41\%$ at 753 K) is observed only in the case of cerium ($XC_3° = 4.5\%$, $SC_3^{=} = 47.2\ \%$, at 753 K). In the presence of lanthanum, propane conversion ($XC_3° = 1.9\%$, at 753 K) and propene selectivity ($SC_3^{=} = 37\%$, at 753 K) are essentially unchanged. Incorporation of praseodymium, samarium or bismuth totally inhibits the formation of propene. And in these catalysts, the increase in propane conversion (fig.IV.12, $XC_3° = 2.8$, 2.1 and 3.2% at 753 K) and oxygen conversion ($XO_2 = 10.7$, 15.5, 12%, respectively at 753 K) only led to an increase of CO_2 yield. Once again, the Tb-modified catalyst is not active at all.

IV.4.2 Catalytic performances of "non-stoichiometric" Ni-Co-Ln(Bi)-Mo-Si (1:1:1:2.5:20)

Table IV.14: Catalytic performances of Ni:Co:Mo:Si (1:1:2.5:20) and Ni:Co:M:Mo:Si (1:1:1:2.5:20) catalysts (M = Bi, La, Ce, Pr, Sm, Tb) in propane ODH.

Ni:Co:M:Mo:Si (M= Ln or Bi)	T (K)	$XC_3°$ (%)	$YC_3^=$ (%)	$SC_3^=$ (%)	XO_2 (%)	$YCO_2/3$ (%)	SCO_2 (%)
M = Bi	**723**	14.5	4.6	31.6	40.8	6.4	43.9
	753	15.2	4.1	26.8	47.8	7.6	49.9
M = La	**723**	15.5	8.0	51.7	40.3	6.7	42.9
	753	15.9	9.1	57.4	44.3	7.2	45.2
M = Ce	**723**	20.7	7.1	34.4	88.5	14.0	67.6
	753	22.2	7.9	35.6	96.1	14.1	63.4
M = Pr	**723**	10.8	6.8	63.3	25.6	4.4	40.5
	753	15.6	9.1	58.3	40.6	6.6	42.1
M = Sm	**723**	6.8	2.5	37.5	25.6	3.4	50.3
	753	9.2	3.8	40.9	29.8	3.9	42.6
M = Tb	**723**	21.3	7.4	34.5	62.8	12.2	57.2
	753	26.4	10.0	37.9	74.5	14.3	54.3
Ni :Co :Mo :Si	**723**	6.8	3.5	51.4	13.7	1.7	24.8
	753	11.5	5.4	47.4	22.9	2.8	24.8

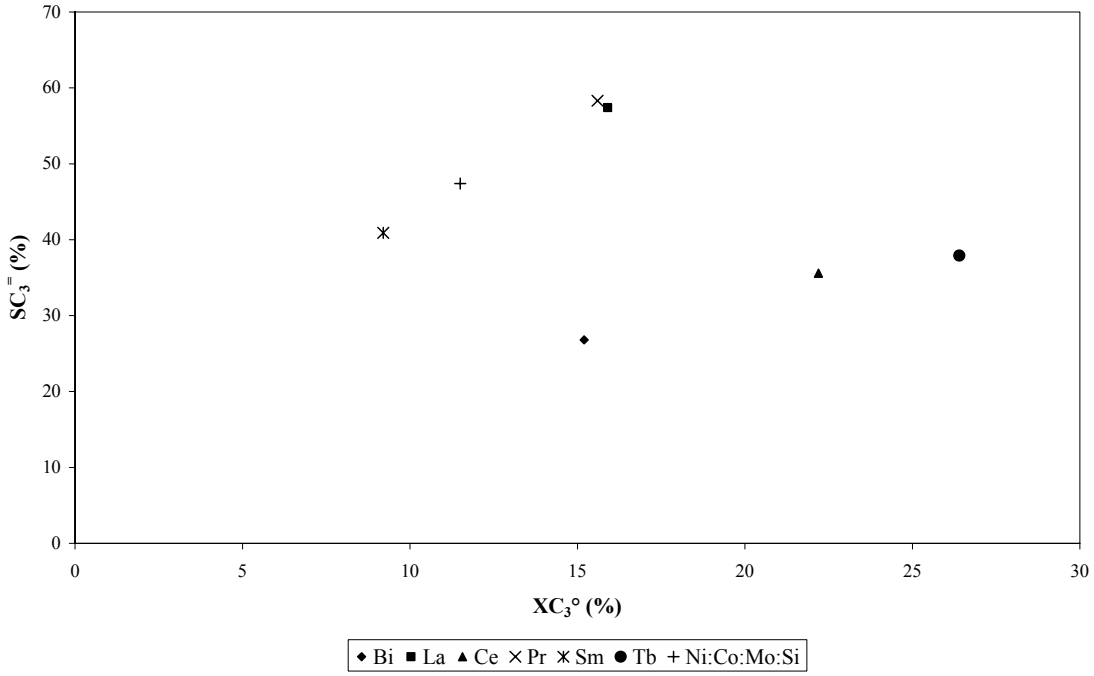

Fig.IV.13: Selectivity to propene from propane as a function of hydrocarbon conversion for all Ni:Co:Ln(Bi):Mo:Si catalysts (at 753 K).

Fig.IV.13 illustrates the selectivity-conversion relationships for all Ni:Co:Ln:Mo:Si catalysts at 753 K. The negative effect of Sm, as additional element, on the catalytic behaviour of Ni:Co:Mo:Si catalyst is quite obvious: this modified catalyst

leads to lower $XC_3°$ and $SC_3^=$ than the initial Ni:Co:Mo:Si system. Even if the Bi-modified catalyst shows a quite positive effect towards propane conversion, the propene selectivity undergoes a strong decrease. In all other cases the catalytic performances are globally enhanced.

IV.4.3 Catalytic performances of "non-stoichiometric" Ni-Co-M-M'(Bi)-Mo-Si (1:1:1:1:2.5:20)

Table IV.15: Catalytic performances of Ni:Co:M:M':Mo:Si catalysts (M = Bi, La, Ce, Pr, Sm, Tb) (1 :1 :1 :1 :2.5 :20) in propane ODH.

Catalysts	T (K)	$XC_3°$ (%)	$YC_3^=$ (%)	$SC_3^=$ (%)	XO_2 (%)	$YCO_2/3$ (%)	SCO_2 (%)
M = La	**723**	9.3	6.2	66.6	35.9	5.5	59.2
M'= Ce	**753**	13.3	6.7	50.5	45.2	6.8	51.0
M = La	**723**	12.5	5.1	40.8	23.5	2.7	21.8
M'= Pr	**753**	13.1	5.9	45.2	27.7	3.0	23.2
M = Ce	**723**	8.2	3.8	46.0	27.2	3.9	47.7
M'= Pr	**753**	13.5	4.8	35.3	40.0	5.6	41.1
M = La	**723**	9.1	2.1	33.3	25.0	3.5	38.3
M'= Bi	**753**	11.9	2.1	17.3	32.8	4.5	38.0
M = Pr	**723**	8.7	2.7	30.6	25.7	3.5	40.6
M'= Bi	**753**	12.2	3.0	24.4	37.2	5.1	41.8
M = Ce	**723**	14.7	4.9	33.1	45.6	6.2	42.4
M'= Bi	**753**	18.1	4.6	25.4	58.6	8.1	44.9
M= Sm	**723**	7.8	4.7	59.9	20.5	2.7	35.1
M'=La	**753**	8.7	5.7	65.8	24.5	3.1	35.9
M= Sm	**723**	3.6	3.6	52.4	11.5	1.6	46.0
M'= Pr	**753**	7.4	4.8	65.6	18.2	2.4	33.2
M = Sm	**723**	6.8	1.6	23.8	24.3	3.3	48.5
M'= Bi	**753**	9.4	1.8	19.0	35.5	5.1	53.9
M = Sm	**723**	8.7	4.8	55.4	25.3	3.6	41.3
M'= Ce	**753**	12.3	6.1	49.6	34.5	5.1	41.7
M = Tb *	**723**	11.0	4.7	42.5	30.1	5.8	52.5
M'= Ce	**753**	21.5	6.9	31.9	62.8	10.2	47.5
M = Tb	**723**	20.6	8.1	39.5	42.4	9.1	44.0
M'= La	**753**	28.2	11.2	39.8	68.9	14.3	50.7
M = Tb	**723**	19.8	7.7	39.0	39.4	8.5	40.5
M'= Pr	**753**	25.7	11.4	44.3	62.5	13.2	51.3
M = Tb	**723**	2.6	0.8	29.9	4.7	1.4	53.0
M'= Bi	**753**	5.0	1.4	27.3	8.8	2.7	54.9
M= Tb	**723**	23.6	9.4	39.9	55.2	11.2	47.3
M'=Sm	**753**	32.7	11.9	36.4	86.8	17.6	53.8

* = values obtained with 150 mg catalyst (instead of 250 mg) because of high O_2 conversion.

Main comments on the catalytic data

As previously stated in Ni-Co-Ln(Bi)-Mo-Si catalysts, Ce and Tb definitely improve the propane conversion (from 13.3 % of a Ce-La modified sample to 32.7 % as

displayed by a Tb-Sm modified catalyst, at 753 K). Tb-based formulations are always characterized by higher $XC_3°$ and XO_2 values than Ce-based catalysts (XO_2 = 86.8, 62.5 and 68.9 % for Tb-Sm, Tb-Pr and Tb-Ce (150 mg), Tb-La respectively, at 753 K).

For all Tb- and Ce-based catalysts, high oxygen conversion leads to a high CO_2 yields and selectivity.

Even if Tb deeply influences the catalytic behaviour of mixed Ni-Co molybdates, the overall catalytic properties of the catalyst in which Tb is involved together with Bi seems to follow completely the intrinsic behaviour of Bi-based catalyst, i.e. very low $XC_3°$ and $SC_3^=$ values.

The Tb-Sm-modified catalyst is the one who displaying the highest $XC_3°$, $YC_3^=$, XO_2 and $YCO_2/3$ values (32.7, 11.9, 86.8 and 17.6% respectively, at 753 K). But Sm does not exert any role in enhancing the selectivity towards propene, which remains quite low (36.4 % at 753 K).

Although less active than the Tb-Sm and Tb-Ce modified catalysts, Tb-La and Tb-Pr systems display a very high activity ($XC_3°$ = 26-28%), higher than those catalysts modified by La or Pr only ($XC_3°$ = 16%); the Tb-Pr combination is also more selective ($SC_3^=$ = 44%) than the Tb-only system ($SC_3^=$ = 38%).

In Ni-Co-Ln-Mo-Si we already noted that the presence of La or Pr allows an enhancement of $SC_3^=$ and that Sm leads to a lower $XC_3°$. When Sm and La or Pr are both involved in the formulation of a mixed Ni-Co molybdate, a decrease of the catalytic activity (surely due to the presence of Sm) is observed when comparing with that of Ln- or Pr- modified catalysts, while $SC_3^=$ is increased compared to that of Ni-Co-Sm-Mo-Si catalyst, due to the presence of La or Pr ($SC_3^= \approx 66\%$).

When Bi is present together with Ce, La, Pr or Sm, the catalyst displays a low selectivity towards propene (≤ 25%); the Sm-Bi combination also results in a low $XC_3°$, which was already a characteristic of the simple Ni-Co-Sm-Mo-Si system.

Ce-Pr and La-Ce-modified Ni-Co molybdates were mutually conceived in order to display high catalytic activity in terms of $XC_3°$ and XO_2, as expected by the presence

of Ce, and high selectivity towards propene because of the presence of La or Pr. However, these catalysts were characterized by a moderate catalytic activity but also an enhanced propene selectivity when compared to that displayed by Ni-Co-Ce-Mo-Si.

Comparison at isoconversion

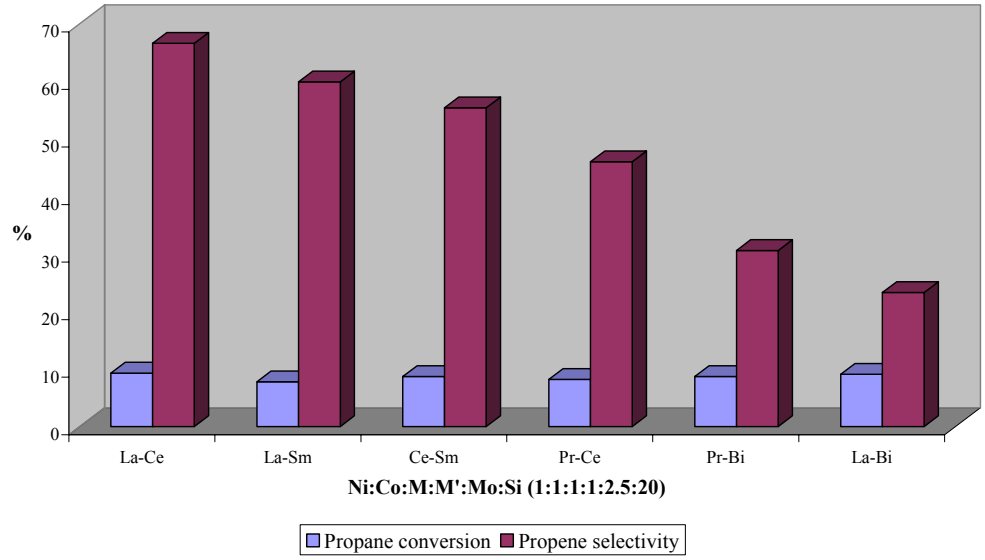

Fig.IV.14: Propane conversion and propene selectivity of some Ni:Co:Ln:Ln'(Bi):Mo:Si, at 723 K.

Selectivity-conversion relationship in Ni:Co:Ln:Ln':Mo:Si catalysts

Fig.IV.15 displays the selectivity-conversion relationships in all multimodified Ni-Co molybdates at 753 K. It comes out that the Sm-La and Sm-Pr associations have a strong positive effect on propene selectivity despite a little decrease in propane conversion. Furthermore, while associations like Sm-Ce, Ce-Pr, La-Pr and La-Ce slightly improve the catalytic performances in comparison to a non-modified Ni:Co:Mo:Si catalyst, the presence of Tb in the formulation always leads to more performing systems

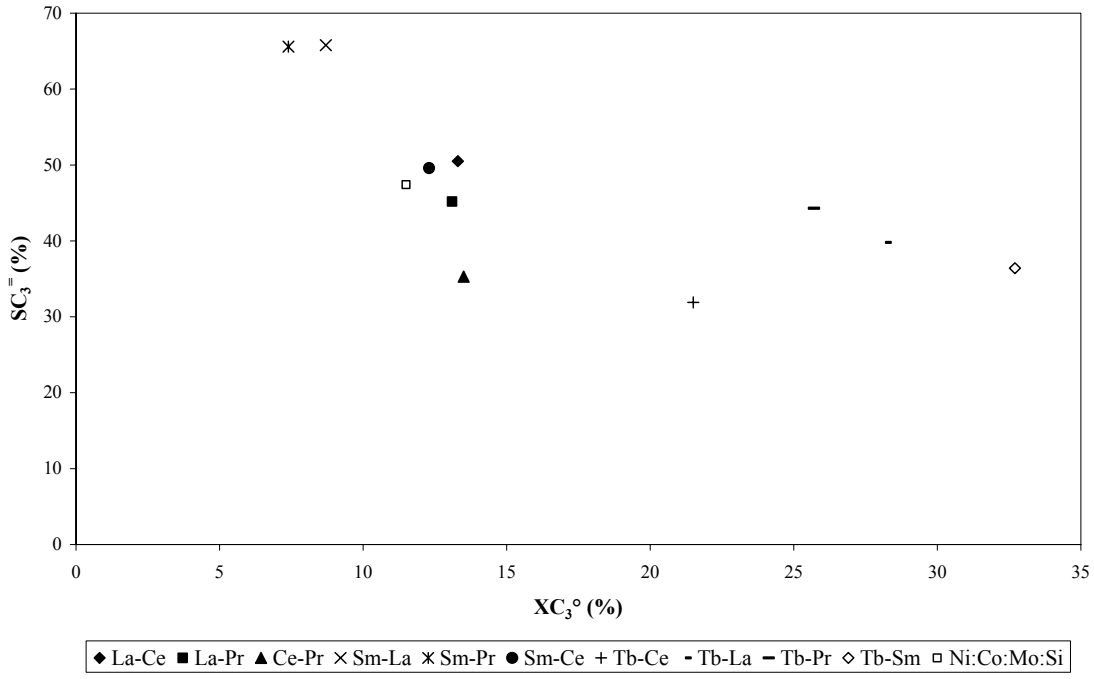

Fig.IV.15: Selectivity to propene from propane as a function of hydrocarbon conversion for all Ni:Co:Ln:Ln':Mo:Si catalysts (T = 753 K).

IV.5 Characterization of used catalysts

IV.5.1 X-ray diffraction

Some tested catalysts have been characterized by XRD and XPS in order to observe eventual changes of crystalline phases and surface compositions during the catalytic tests. In all used catalysts, the crystalline phases are the same as before the catalytic tests: the only difference between the fresh and the used catalysts being a lower degree of crystallinity in the used catalysts.

IV.5.2 X-ray photoelectron spectroscopy

The binding energies of the various elements present in used Ni-Co-Ln-Ln'(Bi)-Mo-Si were found in the following ranges: 856.2 ± 0.3 eV for Ni $2p_{3/2}$, 781.3 ± 0.1 eV for Co $2p_{3/2}$, 232.6 ± 0.1 eV for Mo $3d_{5/2}$, 159.7 ± 0.1 eV for Bi $4f_{7/2}$, 835.5 ± 0.4 eV for La $3d_{5/2}$, 934.4 ± 0.2 eV for Pr $3d_{5/2}$, 900.8 ± 0.2 eV for Ce $3d_{3/2}$, 1083.6 ± 0.1 eV for Sm $3d_{5/2}$, 531.2 ± 0.3 for O(I)1s, 532.9 ± 0.1 for O(II)1s, 103.5 ± 0.2 eV for Si 2p. All binding energies of used catalysts are characterized by values very close to those of the fresh catalysts, with the only exception of the O(I) oxygen component O(I) assigned to

lattice oxygen, which is slightly shifted towards higher binding energy values in used catalysts. In the used catalysts, the O(II) component of the oxygen peak, which lies at higher binding energy and it is assigned to the hydroxyl and carbonate groups which are formed on the surface, is characterized by higher intensity than in the fresh catalysts, allowing us to affirm that some CO_2, produced during the catalytic tests, could be adsorbed on the surface of these catalysts.

Table IV.16 lists XPS results of some multimodified mixed Ni and Co molybdates after the catalytic test. The fact that the experimental (Ni,Co/Mo) ratios of the used catalysts are higher than those of the fresh catalysts, meaning that the surface of tested catalysts is richer in Ni and Co and poorer in Mo is to put in relationship with the possible loss of Mo upon partial volatilisation of MoO_3, during the catalytic reaction. In the same way (M,M'/Mo) of used catalysts are higher than those of fresh catalysts: Ln and Bi are definitely more easily detected on used than on fresh catalysts, and even more than Ni or Co (((Ni,Co/M) and (Ni,Co/M'))$_{used}$ < ((Ni,Co/M) and (Ni,Co/M'))$_{fresh}$).

Table IV.17 shows the carbon percentages of some multimodified Ni-Co molybdates before and after their use in propane ODH. Among all tested catalysts investigated, only two showed a higher carbon content after catalytic test. No significant coke deposition and even, in some cases, removal of initial carbon residual contamination by burning off during the highly exothermal reaction, is observed.

Table IV.16: XPS results of Ni:Co:M:M':Mo:Si (1:1:1:1:2.5:20) samples prepared by the sol-gel method and calcined at 773 K. (Used catalysts)

Ni:Co:M:M':Mo:Si 1 : 1 : 1 : 1 : 2.5 : 20	Ni/Mo Co/Mo		M/Mo M'/Mo		Ni/M Co/M		Ni/M' Co/M'		Ni/Si Co/Si		M/Si M'/Si		Mo/Si		Co/Ni		M/M'	
	Exp	Th	Exp	Th	Exp	Th	Exp	Th	Exp	Th	Exp	Th	Exp	Th	Exp	Th	Exp	Th
M = La M'= Ce	0.14 0.20	0.4 0.4	0.11 0.05	0.4 0.4	1.25 1.82	1 1	2.93 4.26	1 1	0.035 0.051	0.05 0.05	0.028 0.012	0.05 0.05	0.24	0.125	1.46	1	2.3	1
M = La M'= Pr	0.12 0.17	0.4 0.4	0.12 0.10	0.4 0.4	1.02 1.45	1 1	1.2 1.7	1 1	0.022 0.03	0.05 0.05	0.022 0.018	0.05 0.05	0.18	0.125	1.43	1	1.2	1
M = Ce M'= Pr	0.12 0.09	0.4 0.4	0.10 0.13	0.4 0.4	1.25 0.92	1 1	0.92 0.67	1 1	0.018 0.013	0.05 0.05	0.014 0.020	0.05 0.05	0.15	0.125	0.73	1	0.7	1
M = Sm M'= La	0.125 0.23	0.4 0.4	0.10 0.18	0.4 0.4	1.20 2.2	1 1	0.68 1.25	1 1	0.02 0.035	0.05 0.05	0.016 0.027	0.05 0.05	0.15	0.125	2.2	1	0.57	1
M = Sm M'= Ce	0.12 0.17	0.4 0.4	0.07 0.07	0.4 0.4	1.64 2.32	1 1	1.7 2.41	1 1	0.018 0.025	0.05 0.05	0.011 0.015	0.05 0.05	0.14	0.125	1.41	1	1.03	1
M = La M'= Bi	0.106 0.15	0.4 0.4	0.18 0.19	0.4 0.4	0.6 0.85	1 1	0.55 0.80	1 1	0.011 0.016	0.05 0.05	0.019 0.020	0.05 0.05	0.11	0.125	1.44	1	0.93	1
M = Pr M'= Bi	0.25 0.18	0.4 0.4	0.24 0.29	0.4 0.4	1.05 0.76	1 1	0.88 0.63	1 1	0.014 0.010	0.05 0.05	0.013 0.016	0.05 0.05	0.055	0.125	0.72	1	0.84	1

Table IV.17: Carbon percentages in some Ni:Co:M:M':Mo:Si before and after the catalytic test.

Composition and Molar Ratio		Before Catalytic Test	After Catalytic Test
Ni:Co:La:Ce:Mo:Si	1 :1 :1 :1 :2.5 :20	7.2 %	9.0 %
Ni:Co:La:Pr:Mo:Si	1 :1 :1 :1 :2.5 :20	8.6 %	7.4 %
Ni:Co:Ce:Pr:Mo:Si	1 :1 :1 :1 :2.5 :20	9.1 %	4.9 %
Ni:Co:La:Bi:Mo:Si	1 :1 :1 :1 :2.5 :20	6.6 %	6.3 %
Ni:Co:Pr:Bi:Mo:Si	1 :1 :1 :1 :2.5 :20	4.9 %	6.2 %
Ni:Co:Sm:La:Mo:Si	1 :1 :1 :1 :2.5 :20	10.7 %	8.1 %
Ni:Co:Sm:Ce:Mo:Si	1 :1 :1 :1 :2.5 :20	8.6 %	6.6 %

IV.6 On the catalytic performances of Ni and Co molybdates modified by bismuth and/or lanthanides

Industrial selective oxidation catalysts often include in their formulation, besides the main components, which constitute the active phase, a wide range of promoters. These additional elements are supposed to exert a positive effect on the activity, selectivity or durability of the catalyst, even if the mechanism of their action is sometimes unknown. In the next section, we will try to give an explanation for the role of lanthanides as modifying elements in nickel and/or cobalt molybdates.

IV.6.1 Explanation of the catalytic behaviour of modified Ni or Co molybdates (Ni(Co):Ln(Bi):Mo:Si, 1:1:2.5:20) by the hypothesis of a single multicomponent phase

Klissurski (181) showed the rates of exchange of molecular oxygen with the lattices lanthanide oxides (Ln_xO_y); because these rates were particularly high and reached a maximum with praseodymium oxide, he concluded that for weakly and highly reactive oxygen in the surface layer of the catalysts, the oxidation leads mainly to products of complete oxidation. If we consider the lanthanide molybdates, the situation is very different. When referring to the rates and the activation energies (A.E.) for the exchange of oxygen in $C^{18}O_2$ with the oxygen atoms of the corresponding Ln molybdate, it appears that the reactivity of surface oxygen in most molybdates varies very slightly ($56.5 < A.E. < 64.85$ kJ mol^{-1} going from La- to Nd-molybdate). However, the mobility of the oxygen atoms in oxides is higher than in the corresponding molybdates; partial oxidation is therefore more probable on the Ln molybdates because of the lower reactivity of their surface oxygens. If we take into account the activation energies of exchange in pure nickel and cobalt molybdates (213.4 and 224.7 kJ mol^{-1} respectively), they are much higher than those of Ln molybdates, meaning that the former phases are less active but more selective. On the basis of these observations, it could be thought that combining both nickel or cobalt molybdate with a lanthanide molybdate, and eventually preparing them by sol-gel method, which is normally an adequate method to achieve a good dispersion of an active phase on a support, would provide catalysts with improved activity and selectivity.

Keeping in mind this idea, we first prepared, characterized and tested Ni-Mo-Si- and Co-Mo-Si-catalysts (calcined at 1073 K). These catalysts display a low catalytic

activity (table III.1 in Appendix III): Ni-Mo-Si-sample is more active and more selective towards propene than Co-Mo-Si. The experimental atomic ratios (Ni/Si) and (Co/Si) (0.0077 and 0.0025, respectively) show that Ni is better dispersed on silica than Co. Moreover the experimental (Mo/Si) for Ni-Mo-Si-sample (0.0038) and that of Co-Mo-Si-sample (0.0019) suggest that in Ni-molybdate molybdenum is better dispersed than in Co-molybdate. The XPS data suggest that two phases are present on the surface of Ni-Mo-Si (1:1:20) calcined at 1073 K: $NiMoO_4$ and NiO but the latter phase has not been revealed by XRD.

If we compare these catalysts to the modified ones, we observe that the catalytic behaviour of Ln(Bi) modified Ni(Co)-molybdates is very different from that of simple Ni or Co molybdate. We have already underlined the role played by lanthanide oxides towards total oxidation and mentioned that one way to explain their catalytic behaviour is to take into account the reactivity and the mobility of the oxygen atoms present in the lattice of the oxide.

Even if the activation energies of oxygen exchange for nickel and cobalt molybdates are higher than those of Ln molybdates, the modified catalysts displayed low activity and very low selectivity towards propene, the only observed product being in many cases CO_2. Only the Ce- and La-modified Co molybdates improved the intrinsic propene yield. Generally speaking, the lanthanides added to the formulation of the catalysts did not improve their catalytic activity and led to total oxidation products.

The active sites in those molybdates are composed of A-O-Mo-O moieties and it can be assumed that the largest concentrations of those moieties are found on the surface of compounds characterized by stoichiometric compositions (70). This would therefore be the case in this series of catalysts (Ni(Co)-Ln(Bi)-Mo-Si (1:1:2.5:20) = $Ni(Co)MoO_4$ + $Ln(Bi)_2Mo_3O_{12}$). We mentioned above that a quaternary phase, X, was observed by XRD and Raman spectroscopy, resulting from the incorporation of the lanthanide element in the lattice of Ni(Co) molybdate. Only in the case of Ni(Co)-Ce(Bi)-Mo-Si-samples, a mixture of two phases has been identified, namely $Ni(Co)MoO_4$ with CeO_2 or $Bi_2Mo_2O_9$. CeO_2 and $Bi_2Mo_2O_9$ were also prepared by the sol-gel method and tested in propane ODH under the same reaction conditions, but they did not show any catalytic activity.

The quaternary phase, which is the combination of all the elements involved in the catalyst, is not active in propane ODH. This phase is characterized by different types of oxygen, one being related to Ni(Co)-O-Mo-O moieties, and the other one to Ln-O-

Mo-O moieties. We can suppose that the quaternary phase strongly decreases the mobility of oxygens, and that the only "mobile" oxygens (with a reduced mobility, because they are part of a quaternary phase) on the surface are those involved in Ln(Bi)-O-Mo-O moieties (XPS revealed a major presence of Ln on the surface of the catalysts rather than Ni or Co, see table IV.5), which are responsible for the formation of overoxidation products. In the case of Co-La-Mo-Si- and Co-Ce-Mo-Si-samples a way to explain the positive observed catalytic results is to take into account the presence of mixed moieties such as: Co-O-Ln-O which could lead to better catalytic performances and higher selectivities towards propene.

Moriceau and coworkers (182) investigated the catalytic performances of Ni-Ce-based catalysts in propane ODH and claimed the presence of mixed Ni-O-Ce-O moieties, which would modify the properties of Ni-O-Ni species normally present in NiO. These moieties seem to exert a positive influence on the global catalytic behaviour of the catalyst. In our case Co-O-Ln-O might be formed only in the Co-La-Mo-Si and Co-Ce-Mo-Si systems, leading to enhanced catalytic performances. Moreover, in our case, the presence of a second quaternary phase (M^{2+} ions incorporated in $Ln_2Mo_3O_{12}$) could also play a role in the catalytic activity. Further studies would be necessary to elucidate the occurrence and the cause of an eventual synergetic effect.

IV.6.2 On the catalytic behaviour of modified mixed Ni and Co molybdates (Ni:Co:Ln(Bi):Mo:Si, 1:1:1:2.5:20)

When foreign elements are incorporated as dopants in a host oxide lattice, most of its electronic and structural characteristics can in principle be modified: acid-base and redox character, mobility of oxygen, electronic conductivity and vacancies concentration. Furthermore, when several crystalline phases are present simultaneously, additional phenomena related to the interfaces and leading occasionally to phase cooperation can also occur.

Table IV.18*:* Ionization energy, absolute hardness and redox potential of the lanthanides and bismuth present in modified Ni and Co molybdates.

Cations	Redox Couple	Ionization Energy I (eV)	Absolute Hardness η (eV)	Standard Redox Potential E° (V)
La^{3+}	La^{3+}/La	49.95	15.38	-2.38
Ce^{4+}	Ce^{4+}/Ce^{3+}	65.55	14.39	1.72
Pr^{3+}	Pr^{3+}/Pr	38.98	8.68	-2.35
Sm^{3+}	Sm^{3+}/Sm^{2+}	41.40	9.00	-1.55
Tb^{4+}	Tb^{4+}/Tb^{3+}	66.46	13.33	3.01
Bi^{3+}	Bi^{3+}/Bi	45.92	9.86	0.317

IV.6.2.1 Heat of formation of the oxides

Morooka et al (183) measured the catalytic activity of a variety of oxides in the oxidation of several hydrocarbons and found a good correlation between the catalytic activity and the standard formation enthalpy of the oxide per mol of oxygen. These normalized ΔH^0_f values of the different sesquioxides (Ln_2O_3) are not really different from each other, and those of higher oxides (LnO_x, x>1.5) are lower than those of the sesquioxides (fig. IV.16). These observations were used by Hattori (115) to explain the difference in the catalytic behaviour between these two types of oxides, but could not be used to interpret the differences among the higher oxides or among the sesquioxides.

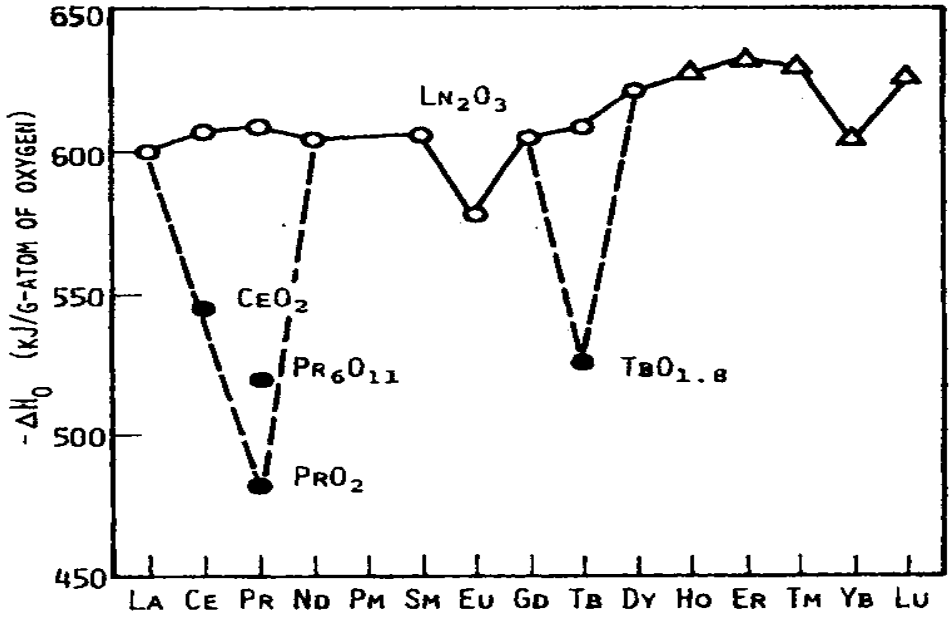

Fig.IV.16: Heat of formation of lanthanide oxide per g-atom of oxygen (115).

In our case, even if we did not detect any Ln_2O_3 oxide or TbO_2 by XRD, we identified the presence of CeO_2 and we suppose that the lanthanides introduced in the Ni:Co:Ln:Mo:Si catalysts must be essentially present as such oxides. Plotting the ΔH^0_f of these oxides against the $YCO_2/3$ values, we observed that the lower (in absolute value) the heat of formation of the oxide, the higher the catalytic activity (table IV.19 and fig. IV.17). The same correlation is also observed when looking at the intrinsic CO_2 yields ($Y*CO_2/3$). This correlation led us to conclude that the most active catalysts are

those containing Ce and Tb oxides and that the catalytic performances is mainly due to the presence of tetravalent ions.

Table VI.19: Comparison between the standard formation enthalpies (at 298 K) of lanthanide oxides present in Ni:Co:Ln:Mo:Si catalysts and their respective $YCO_2/3$ values at 753 K.

Catalyst	Oxides	ΔH^0_f (kJ mol^{-1})	$YCO_2/3$ (%)
Ni:Co:La:Mo:Si	La_2O_3	-1792.8	7.2
Ni:Co:Ce:Mo:Si	CeO_2	-1088.7	14.1
Ni:Co:Pr:Mo:Si	Pr_2O_3	-1809.6	6.6
Ni:Co:Sm:Mo:Si	Sm_2O3	-1823.0	3.9
Ni:Co:Tb:Mo:Si	TbO_2	-971.5	14.3

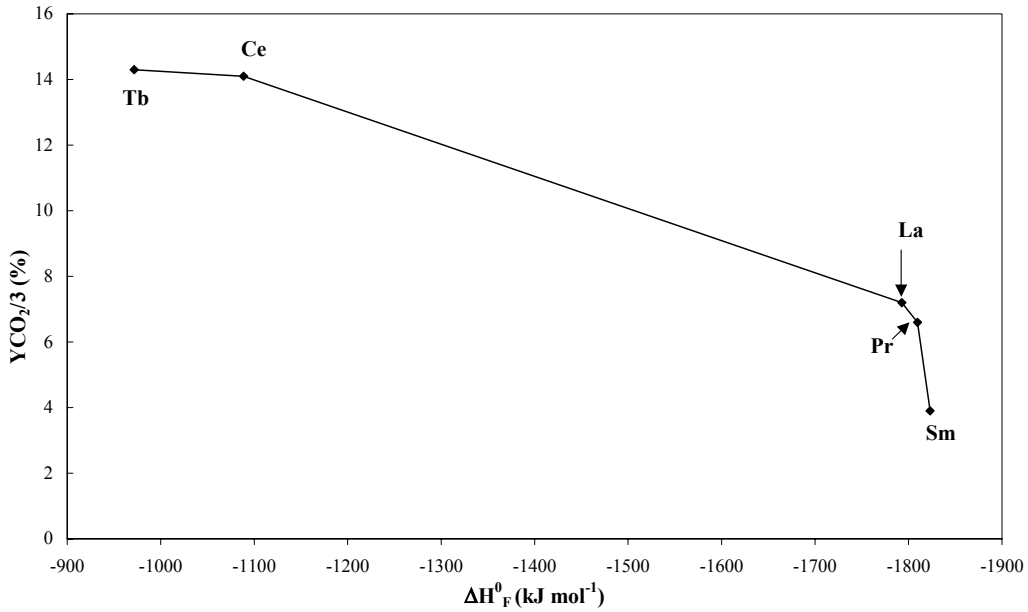

Fig.VI.17: Evolution of the CO_2 yields of Ni:Co:Ln:Mo:Si (1:1:1:2.5:20) catalysts with respect to the standard formation enthalpies of the Ln oxides incorporated.

This kind of correlation, which is almost qualitative, allows to attribute the catalytic activity to the stability of the tetravalent ion. In the past, the oxidation of CO on CeO_2 was interpreted by Hattori (115) by the two following steps:

$2\ Ln^{4+} + O^{2-} + CO \rightarrow 2\ Ln^{3+} + CO_2$

$2\ Ln^{3+} + ½\ O_2 \rightarrow 2\ Ln^{4+} + O^{2-}$

The overall reaction was found to depend on the ease of oxidation of the trivalent ion (major effect on a highly reduced catalyst) and on the ease of reduction of the tetravalent ion (major effect on a highly oxidized catalyst). Taking into account all these ideas, Hattori attributed the catalytic activity of the lanthanide oxides under reducing atmosphere to the relative stability of the tetravalent ion compared to the trivalent state.

IV.6.2.2 Absolute hardness

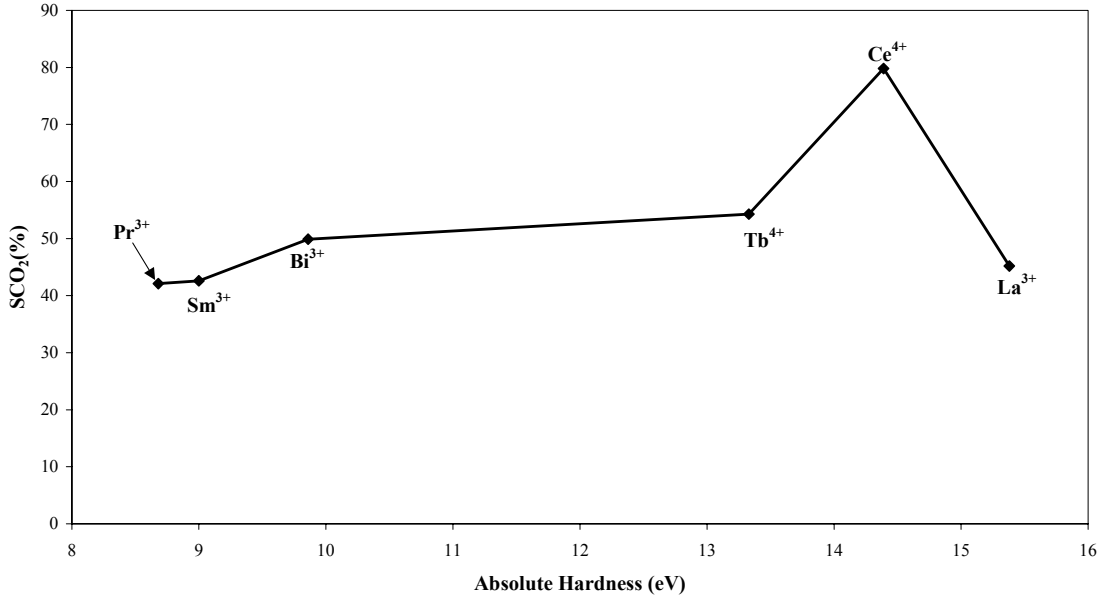

Fig.IV.18: Evolution of the CO_2 selectivity with respect to the absolute hardness of the additional elements.

IV.6.2.3 Redox potential

The heat of reoxidation measures the energy released when two metal-oxygen bonds are formed in the solid. Kung et al (39) demonstrated that there is a strong correlation between the selectivity for oxidative dehydrogenation of butane and the heat of reoxidation of V_2O_5/γ-Al_2O_3 catalyst. Selectivity is low when the reoxidation heat is low but increases rapidly with this parameter.

The concept was tested using a series of orthovanadates ($M_3(VO_4)_2$ and MVO_4). The cations in these two series were chosen in order to have a range of reduction potentials from –2.40 V and +0.77 V. In these structures there are only M-O-V bonds and no V-O-V bonds and the difference in the ease of removal of a lattice oxygen should depend on the difference in the reduction potential of the M ion. When plotting the reduction potential of the cations against the selectivity for ODH, a correlation

appears: the higher the reduction potential (the more easily reduced the cation), the lower the selectivity.

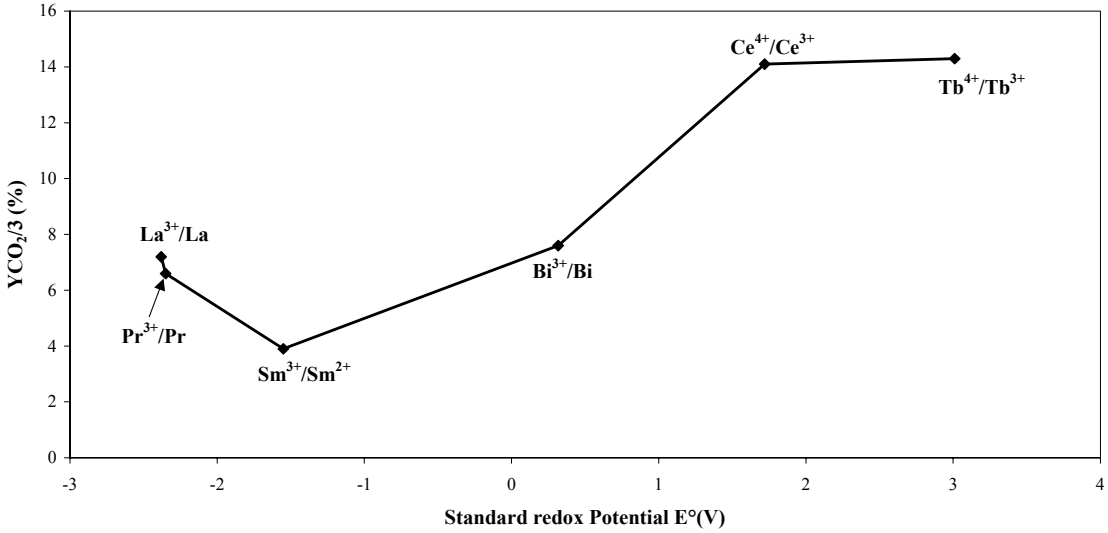

Fig.IV.19: Evolution of the CO_2 yield with respect to the standard redox potential of the additional elements.

IV.6.3 On the catalytic behaviour of multi-modified mixed Ni and Co molybdates (Ni:Co:Ln:Ln':Mo:Si, 1:1:1:1:2.5:20)

Table IV.20: Calculated average ionization energy, average absolute hardness and average redox potential of the lanthanides present in multimodified Ni and Co molybdates.

Lanthanides involved in catalyst formulation	Redox couples	Average ionisation energy (eV)	Average absolute hardness (eV)	Average redox potential (V)
Tb-La	Tb^{4+}/Tb^{3+} La^{3+}/La	58.21	14.36	0.315
Tb-Ce	Tb^{4+}/Tb^{3+} Ce^{4+}/Ce^{3+}	66.0	13.86	2.37
La-Ce	La^{3+}/La Ce^{4+}/Ce^{3+}	57.75	14.885	-0.33
Tb-Sm	Tb^{4+}/Tb^{3+} Sm^{3+}/Sm^{2+}	53.93	11.17	0.73
Sm-Ce	Sm^{3+}/Sm^{2+} Ce^{4+}/Ce^{3+}	53.47	11.695	0.085
Tb-Pr	Tb^{4+}/Tb^{3+} Pr^{3+}/Pr	52.72	11.0	0.33
Ce-Pr	Ce^{4+}/Ce^{3+} Pr^{3+}/Pr	52.26	11.535	-0.315
La-Sm	La^{3+}/La Sm^{3+}/Sm^{2+}	45.67	12.19	-1.965
La-Pr	La^{3+}/La Pr^{3+}/Pr	44.46	12.03	-2.365
Pr-Sm	Pr^{3+}/Pr Sm^{3+}/Sm^{2+}	40.19	8.84	-1.95

IV.6.3.1 Ionization energy

This behaviour also accounts for the evolution of the selectivity towards propene with respect to the average IE (fig.IV.20): all Tb-based catalysts are characterized by lower propene selectivities. These very active Tb-Ln catalysts promote total oxidation rather than partial oxidation. This is consistent with the fact that reactive oxygen ions would be mainly located in the vicinity of Tb; the global activity of the catalyst would therefore be mainly influenced by the presence of Tb rather than that of the other lanthanide.

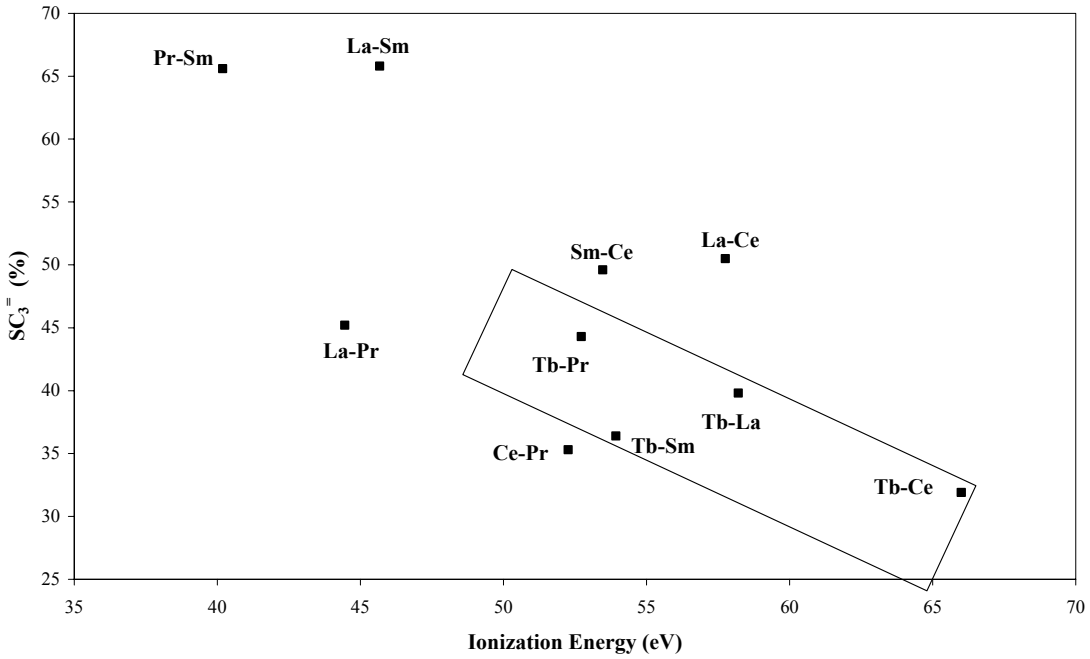

Fig.IV.20: Evolution of propene selectivity of Ni:Co:Ln:Ln':Mo:Si (Ln, Ln' = La, Ce, Pr, Sm, Tb) catalysts with respect to the ionization energy of the additional elements.

IV.6.3.2 Redox potential

Fig.IV.21 shows an interesting correlation between propene selectivity and the average standard redox potential of the lanthanides. As consequence of their high redox potentials, all Tb-Ln modified molybdates, very active in the formation of overoxidation products, are characterized by low propene selectivity values. The high reducibility of Tb-Ln cations promotes the formation of electrophilic oxygen species, responsible for the total oxidation.

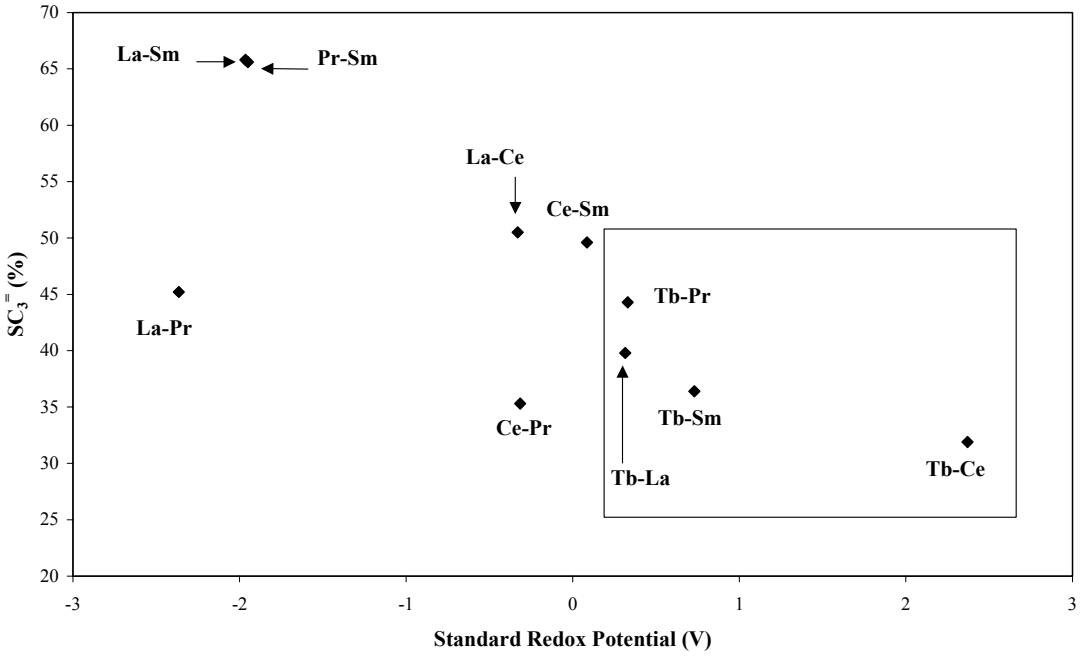

Fig.IV.21: Evolution of propene selectivity of Ni:Co:Ln:Ln':Mo:Si (Ln, Ln' = La, Ce, Pr, Sm, Tb) catalysts with respect to the standard redox potential of the additional elements.